5-2019

Behavior and Energy Loss Optimization of an Elastic Material Metastructure

Andrew S. Montalbano
Clemson University, amonta@g.clemson.edu

Behavior and Energy Loss Optimization of an Elastic Material Metastructure

---

A Thesis
Presented to
the Graduate School of
Clemson University

In Partial Fulfillment
of the Requirements for the Degree
Master of Science
Mechanical Engineering

---

by
Andrew Montalbano
May 2019

Accepted by:
Dr. Georges Fadel, Committee Chair
Dr. Gang Li
Dr. Nicole Coutris

Abstract

Advances in additive manufacturing expand the possibilities of what can be designed and produced. One such example is producing structures that possess designed properties. Because the structure itself has the designed property, it does not require the structure's base material to have it. This allows the use of materials that lack a property to gain that property through geometry. Most elastic materials such as steel do not possess any form of energy loss under loading in their elastic regime. This research asks if a structure made from an elastic material could be designed in such a way to provide energy loss.

One structure of interest is curved-bistable beam switches found in MEMs machines. These switches are of interest because they have different loading and unloading force-displacement curves, resulting in different energy levels between loading and unloading. This results in the system having a hysteresic energy loss. Because individual beams have energy loss, this begs the question if a system of these beams could be designed to produce a structure with energy loss. This structure could then be used to substitute existing systems, such as a suspension system.

The goal of this research is to investigate the behavior and to optimize a structure featuring these curved-bistable beams. On the system level, the deformation pattern, stresses throughout the structure, and total energy loss is calculated. To better understand how the variables of the curved beam affect energy loss, a surrogate model for E_{loss} is produced. This model is then used to optimize both a single beam and a structure of multiple beams. Finally, the material selection's role in optimization is discussed.

Acknowledgements

This project was partially funded by the Automotive Research Center, a U.S. Army center of excellence for modeling and simulation of ground vehicles, led by the University of Michigan College of Engineering. The views presented in this work do not necessarily reflect those of our sponsor, whose support is gratefully appreciated.

Contents

List of Figures

List of Tables

Nomenclature

E	-	Young's Modulus
t	-	thickness of the beam
b	-	depth of the beam
l	-	span of the beam
h	-	height of the beam at the apex
E_{loss}	-	Energy lost by the system
$E_{loading}$	-	Energy put into the system to move to its second stable point
$E_{unloading}$	-	Energy put into the system to move to its initial stable point
0	-	(*subscript*) the initial spring
n	-	number of rows
m	-	number of columns
i	-	(*subscript*) the current column
j	-	(*subscript*) the current row
k	-	stiffness
F	-	Nondimensionalized force
f	-	dimensionalized force
Δ	-	Nondimensionalized displacement
d	-	dimensionalized displacement
x	-	maximum number of springs found in a single row
$A :: B$	-	relates A and B

$A \sim B$	-	A scales with B
$w(x)$	-	shape of the beam
P	-	dimensionless axial load
p	-	dimensionless axial load
N	-	dimensionless normal force
σ_{max}	-	maximum stress felt by the structure under loading
f_n	-	stiffness factor
M	-	moment
t_2	-	leg thickness
h_2	-	leg height
α	-	thickness coefficient
Num.	-	number of springs in a mesh
L_0	-	domain length
H_0	-	domain height
T_0	-	original thickness

Chapter 1

Introduction and Literature Review

1.1 Introduction

All vehicles use some sort of spring-damper system to help level out and smooth the ride. Current systems use a system of springs, either coil or leaf, in tandem with dampeners to provide vibration damping and remove energy from the system in the form of heat and vibrations. Because energy is being removed from the system, these systems can be said to provide energy loss. This research investigates whether these systems could be replaced with a metamaterial or metastructure.

Metamaterials are structures with designed properties originally used in electromagnetic and optical devices [4]. Since their introduction, they have expanded into elastic and thermo applications [11]. At their core, Metamaterials consist of repeated geometric structures. The property that is being modified or added is derived from these geometric structures. For example, [10] produces a metamaterial with a designed

nonlinear deformation response. This is achieved by using cantilever beams meshed together to form a grid. The dimensions of these beams are then optimized to reproduce a targeted nonlinear response [5]. More specifically, this metamaterial matches the loading behavior of rubber.

Speaking of rubber; when rubber is loaded, its loading and unloading paths vary slightly as seen in figure 1.1 [8]. When a system undergoes loading, energy is added into the system causing deformations. Calculating the energy necessary to deform the structure is achieved by integrating underneath the force-displacement curve corresponding to loading. When the system is unloaded, this energy is released from the system. Similar to loading, to find the energy released one can integrate under the force-displacement curve corresponding to unloading. In the rubber's case, its force-displacement curves differ, these integrals also differ. This indicates that there is an energy difference between the loading and unloading curves. The energy lost is the difference between the two areas, highlighted in figure 1.1.

Because matching the loading behavior of rubber is possible, this begs the question if matching rubber's hysteresic energy loss is possible. Previous studies have shown that geometric structures can be used to produce energy loss [3]. This would allow materials that otherwise would not have energy loss, such as steel, to be manufactured in such a way to contain energy loss. This structure could then be optimized in order to provide a specific amount of energy loss.

1.2 Literature Review

One such structure with different loading and unloading behaviors was investigated in [3] and consists of several curved-bistable beams. These beams were originally designed to be used in micro-electro-mechanical systems [9]. [9] explores the behavior

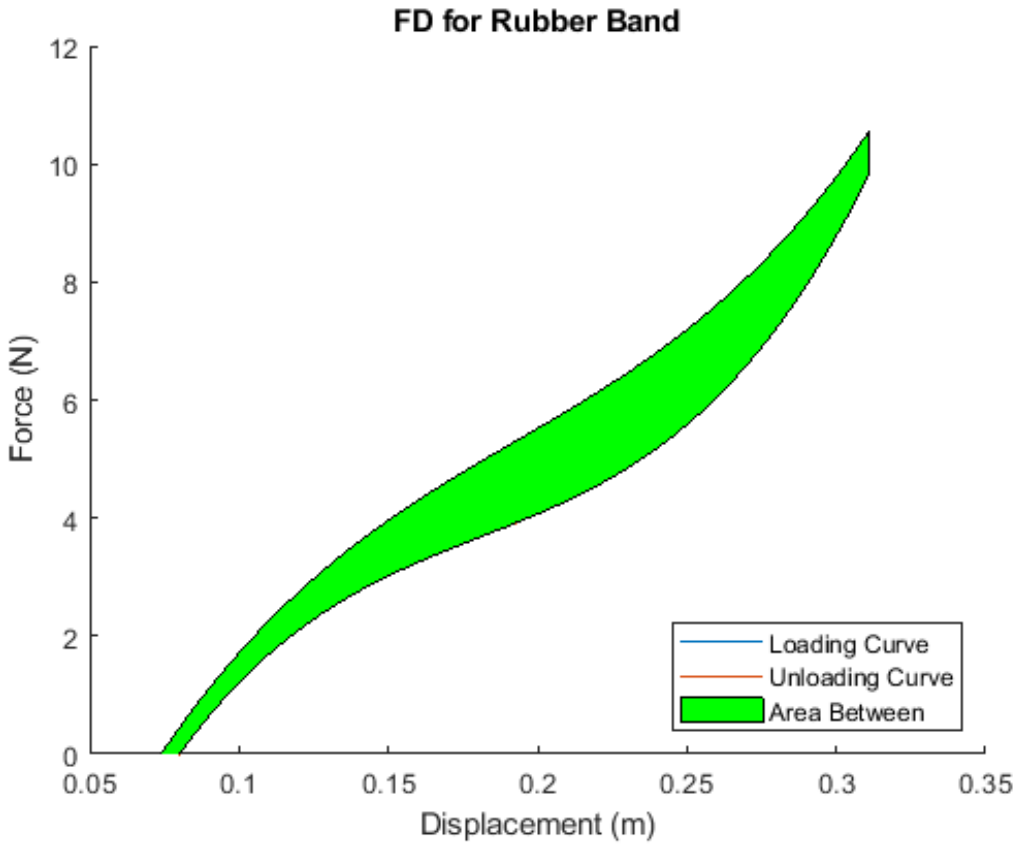

Figure 1.1: Loading and Unloading curves for a Rubber Specimen [8]

of this structure, and derives several of its properties. An example of this structure can be seen in figure 1.2.

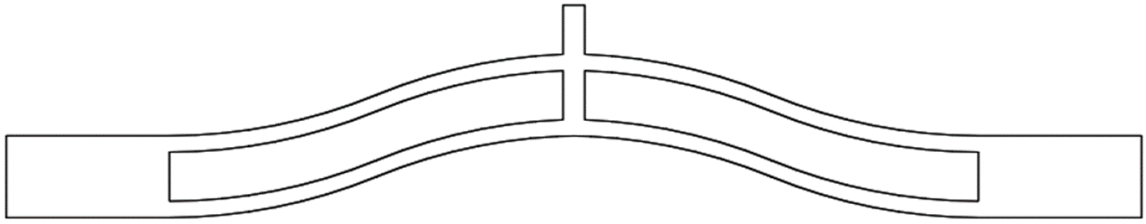

Figure 1.2: Single Cell

Figure 1.2 features two curved beams, connected at their centers. Each beam takes the shape of a cosine curve. From [9], the shape of each beam is given by:

$$y = \frac{h}{2}\Big(1 - \cos(2\pi\frac{x}{l})\Big) \tag{1.1}$$

where h is the height of the apex of the beam and l is the span of the beam. Each beam is t thick, and has a depth of b. x in equation 1.1 ranges from 0 to l. A drawing of this system can be seen in figure 1.3.

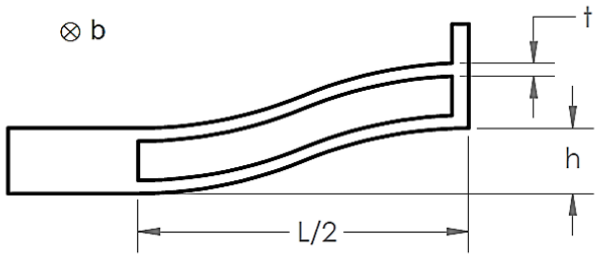

Figure 1.3: Dimensional Diagram

Under most circumstances, the depth of the structure (b) will be larger than its thickness (t). Generally, would indicate the structure is a plate, not a beam. However, previous works modeled the structure as a beam and produced highly accurate results [9][6]. Because of this, in the rest of this document, the structure will be considered to be a beam.

When a beam is being loaded, once the load has surpassed a critical value the beam will buckle. This buckling takes the form of the beam flexing out of its original shape. Generally, systems will buckle in a manner that produces a single flex, referred to as mode 1 buckling. However, under specific circumstances, the system may buckle under higher modes of buckling. Each of these higher modes adds additional 'flexes' to the structure. These modes of buckling for a straight beam can be seen in figure 1.4.

In either figure 1.2 or 1.3 it can be seen that the mechanism has two curved beams connected at the center. Counter to most beams, this beam buckles in mode 3 buckling instead of mode 1 buckling. Because the beam is designed in the shape of mode 1 buckling, it seeks to buckle under the next available mode; mode 2. However, as seen

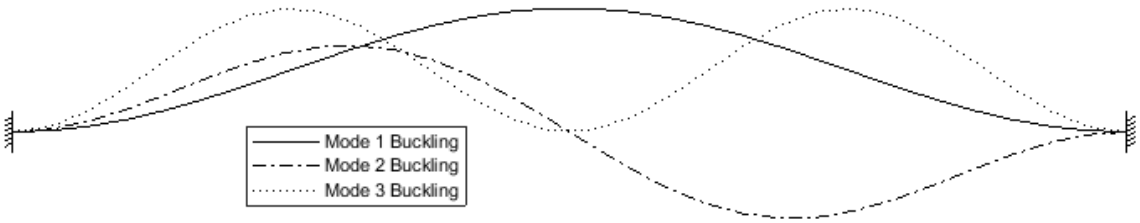

Figure 1.4: Buckling Modes 1 2 & 3

in figure 1.4, mode 2 buckling requires twisting in the center. By adding the center support, this twisting is suppressed. Because of this, the system moves to the next highest buckling, mode 3. Why the removal of mode 2 buckling is necessary will be discussed later in section 1.2.2.

A simple FEA model was constructed to simulate the structure to verify it's snap-through and bistability properties. The shape of the structure is obtained by using equation 1.2 with the following dimensions: $h = 3.0$mm, $t = 0.5$mm, $l = 30$mm, and $b = 10.0$mm. The material chosen was aluminum. The simulation was run as force-controlled, with two rigid plates attached to the top and bottom portions of the structure. The top rigid plate fixes rotation and applies a linearly increasing load, while the bottom has an encaster boundary condition. Finally, the RHS has an x-symmetry boundary condition. These boundary conditions can be seen in figure 1.5.

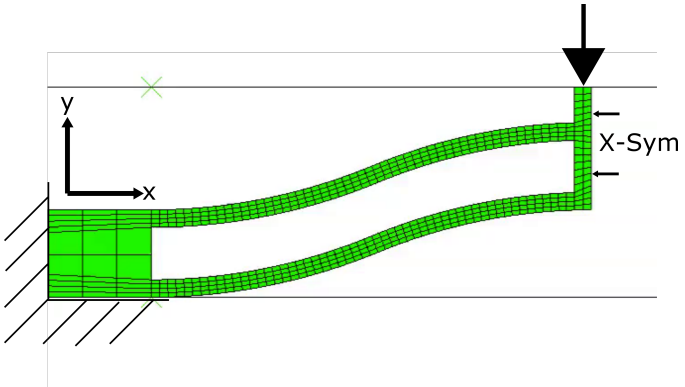

Figure 1.5: Example FEA Boundary Conditions

Extracting several frames from the FEA the snap-through can be seen in figures 1.6-1.8.

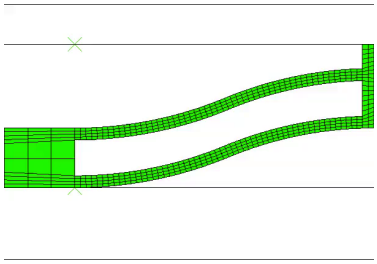

Figure 1.6: Shape A

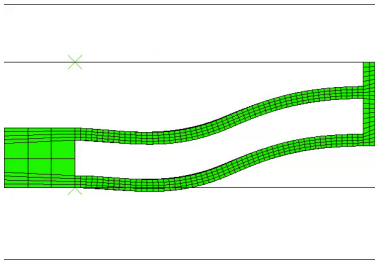

Figure 1.7: Shape B

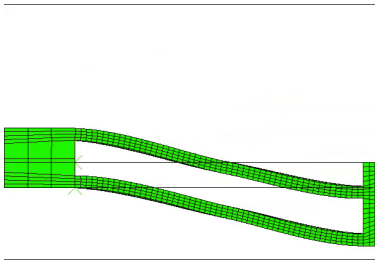

Figure 1.8: Shape C

Shape A shows the system prior to loading. Shape B shows the system just prior to snap-through. Comparing Shape B with the modes of buckling found in figure 1.4, Shape B is undergoing mode 3 buckling. Finally, Shape C shows the beam after it has snapped-through.

The finite element simulation ran for a few seconds post snap-through. Post snap-through the beam undergoes mild vibrations. These vibrations are how the system losses energy.

1.2.1 Theoretical Relations

As mentioned previously, [9] has derived several equations pertaining to these mechanisms. Their paper largely focuses on these structures for use in a MEMs machine [9]. Because of this, their work deals with the forces involved. A later work [6] builds upon the work of [9] and makes more accurate versions of the equations, as well as investigates the force-displacement curves and stress involved.

From [9], the buckling equation of a beam is given by:

$$EI\frac{d^4w}{dx^4} + P\frac{d^2w}{dx^2} = 0 \tag{1.2}$$

The general solution for equation 1.2 has the form of:

$$w(x) = C_1 \sin(kx) + C_2 \cos(kx) + C_3 + C_4 \tag{1.3}$$

where $k = \sqrt{\frac{P}{EI}}$ and C_n are constants.

The bistable beam shape seen in figure 1.3 has clamped-clamped boundary conditions. This makes the boundary conditions of equation 1.3:

$$w(0) = w'(0) = w(l) = w'(l) = 0 \tag{1.4}$$

In order for equation 1.3 to have non-zeros solutions, the dimensionless axial force, N, defined as ${Pl^2}/{EI}$ must satisfy:

$$\sin\left(\frac{N}{2}\right)\left[\tan\left(\frac{N}{2}\right) - \frac{N}{2}\right] = 0 \tag{1.5}$$

Equation 1.5 has an infinite amount of solutions indicating a modal solution:

$$w(x) = \sum_{j=1}^{\infty} a_j w_j(x) \tag{1.6}$$

The index a_j found in equation 1.6 refers to the contribution of each mode, while w_j is the shape of that mode. Breaking equation 1.6 in half, there is:

$$\left.\begin{aligned} w_j(x) &= C(1 - \cos(N_j \tfrac{x}{l}) \\ N_j &= (j+1)\pi \end{aligned}\right\} j = 1, 3, 5... \tag{1.7}$$

which is the solution of the odd modes of buckling, and

$$\left.\begin{aligned} w_j(x) &= C(1-2\tfrac{x}{l}-\cos(N_j\tfrac{x}{l})+2\tfrac{\sin(N_j\frac{x}{l})}{N_j} \\ N_j &= 2.86\pi, 4.92\pi ... \pi \end{aligned}\right\} j = 2,4,6,8... \tag{1.8}$$

which corresponds to the even modes of buckling.

Continuing from equation 1.6, the force-displacement curve for the structure can be obtained. The full derivation of the force-displacement curves may be seen in either [9] or [6]. However, there is an important distinction to be made between the two works; [9] focused on only a single mode of buckling seen in equation 1.6, while [6] investigated this equation with all buckling modes. While the equation with only a single mode has an algebraic solution, it is not very accurate. However, the solution with higher terms, while lacking an algebraic solution, is far more accurate. Because of this, the higher mode solution is used in optimization. To obtain an algebraic solution, the solution with the higher terms is used to produce a surrogate model.

1.2.2 Force-Displacement Curve

From [9], the force-displacement curve of considering only a single term from equation 1.6 is:

$$F = \frac{3}{2}\pi^4 Q^2 \Delta\Big(\Delta^2 - 3\Delta + 2 + \frac{4}{3Q^2}\Big) \tag{1.9}$$

where Δ is $\frac{d}{h}$ and ranges from 0 to 2. d is the displacement being added to the system. When $d = 2h$, the system has fully snapped-through.

With the shape manufactured in mode 1 buckling, when loaded the structure skips mode 1 buckling and seeks to buckle under the next available mode.[9] also provides

the next two buckling modes. These are:

$$F_{Mode2} = 4.18\pi^4 - 2.18\pi^4\Delta \tag{1.10}$$

$$F_{Mode3} = 8\pi^4 - 6\pi^4\Delta \tag{1.11}$$

A graph of equations 1.9, 1.10, and 1.11 can be seen in figure 1.9.

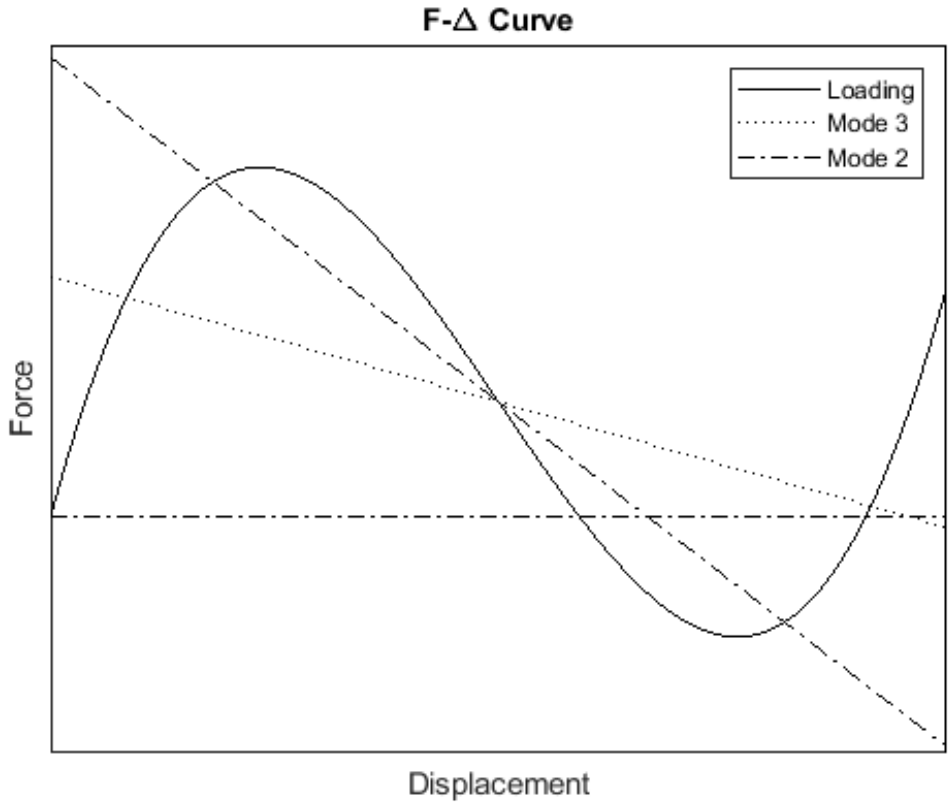

Figure 1.9: Force-Δ Curve with Mode 1 and 2 Buckling

Figure 1.9 shows that each buckling mode intersects the force displacement curve. At these intersections, the system translates from its normal force-displacement curve to the intersected buckling curve. The system continues loading along that path until the buckling mode re-intersects the force-displacement curve. At this instance, normal loading resumes.

Upon closer inspection of figure 1.9, mode 2 buckling intersects the force curve before intersecting the x-axis, where the system continues loading. Because of this, the system lacks a second 0 force point; ie it lacks bistability. Mode 3 intersects the x-axis prior to intersecting the curve. Because of this, it has an intersection with the force curve that occurs below the x-axis. This means that after that intersection, the system follows its original force-displacement curve, and therefore has a zero intersection later along its path. For mode 2, this intersection occurs above the x-axis, and the force curve only continues upward from there. An intersection with the 0-force curve indicates bistability, and its location is the second stable point. This is why the second mode needs to be constrained, while the third mode of buckling does not. Constraining the second mode takes the form of a center connection as seen in figure 1.2. This is why the beam takes the shape of equation 1.1

Returning to the force-displacement solutions; unlike the single mode solution, the force-displacement curve for higher modes lacks a clear algebraic solution. Its solution comes in the form of 2 separate equations. The first relation relates the mechanism's normal (N) and axial forces (F) together.

From [6]:

$$\frac{3}{16N^4}\Big(1+\frac{\tan^2\frac{N}{4}}{3}-\frac{\tan\frac{N}{4}}{\frac{N}{4}}\Big)F^2-\frac{4\pi^2}{(N^2-4\pi^2)^2}F+\frac{N^2}{12Q^2}-\frac{\pi^2N^2(N^2-8\pi^2)^2}{4(N^2-4\pi^2)^2}=0 \quad (1.12)$$

Equation 1.12 is solved by finding the range of N that produces only real solutions in equation 1.12. Once this has been done, the pair of N and F are then sent to equation 1.13 to solve for their corresponding Δ:

$$F=\frac{N^4}{\frac{N}{4}-\tan(\frac{N}{4})}\Big(\frac{N^2}{N^2-4\pi^2}-\Delta\Big) \quad (1.13)$$

To get the $F - \Delta$ for the higher-mode solution, the following algorithm is preformed:

1. Find the range N that equation 1.12 only has real solutions
2. Using the range of N, solve the corresponding F in equation 1.12
3. Use both N and F in 1.13 to solve for their corresponding Δs
4. Dimensionalize N, F, and Δ

Equation 1.12 takes the form of a quadratic leading to two solutions. Each of these solutions forms half of the force-displacement curve; when combined, they complete the force-displacement curve.

As mentioned previously, the single mode is not quite as accurate as of the solution with higher modes. A comparison between theory featuring only a single mode, theory with higher modes, and a finite element analysis can be seen in figure 1.10 with the variables used were: $E = 169\text{GPa}$, $l = 5\text{mm}$, $t = 20\mu\text{m}$, $b = 10\text{mm}$ and $h = 80\mu\text{m}$

It can be seen from figure 1.10 that the higher mode theory is in agreement with the FEA solution. While the single model solution is slightly off.

A quick note about the FEA results seen in figure 1.10: They were obtained by using displacement-control rather than force-controlled. This means the location of the apex of the structure is prescribed at each iteration when solving. Because of this, snap-through does not directly occur when using displacement-control. On the other hand, FEA with force-control would show snap-through. Displacement-control was selected to show mode 3 buckling, and compare the FEA mode 3 buckling to that of the theories. Additionally, due to the suddenness of snap-through, there is a heavy amount of vibrations that obscure the force-displacement curve. Switching from force-control to displacement-control eliminates these vibrations. A discussion

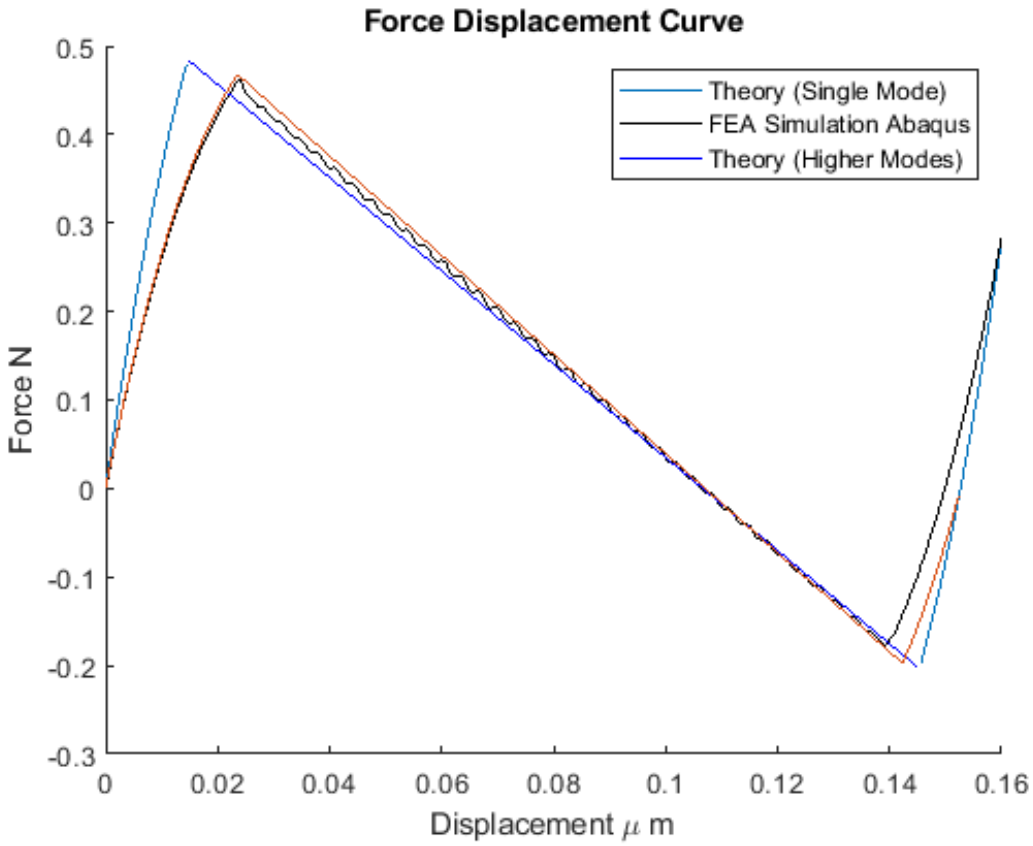

Figure 1.10: f-d Comparison of FEA, Single Mode, and Higher Mode Solutions

of the force-displacement curve is in section 2.1.

Figure 1.10 shows us the force-displacement curve of the curved beam system. Returning to the problem statement, the goal is to find the energy of the system. This is obtained by integrating along the force-displacement curve. Integrating the theoretical curve with higher modes results in the figure seen in figure 1.11. The left curve shows the energy being put into the system; while the right curve shows the energy necessary to go back. Point A in figure 1.11 shows when snap-through happens. As soon as it occurs, no more energy is added into the system as the system moves under its own volition. Likewise, point B shows when snap-back occurs, and the system moves again under its own volition.

The energy as a function of Δ can be explained by using a business card. Flexing

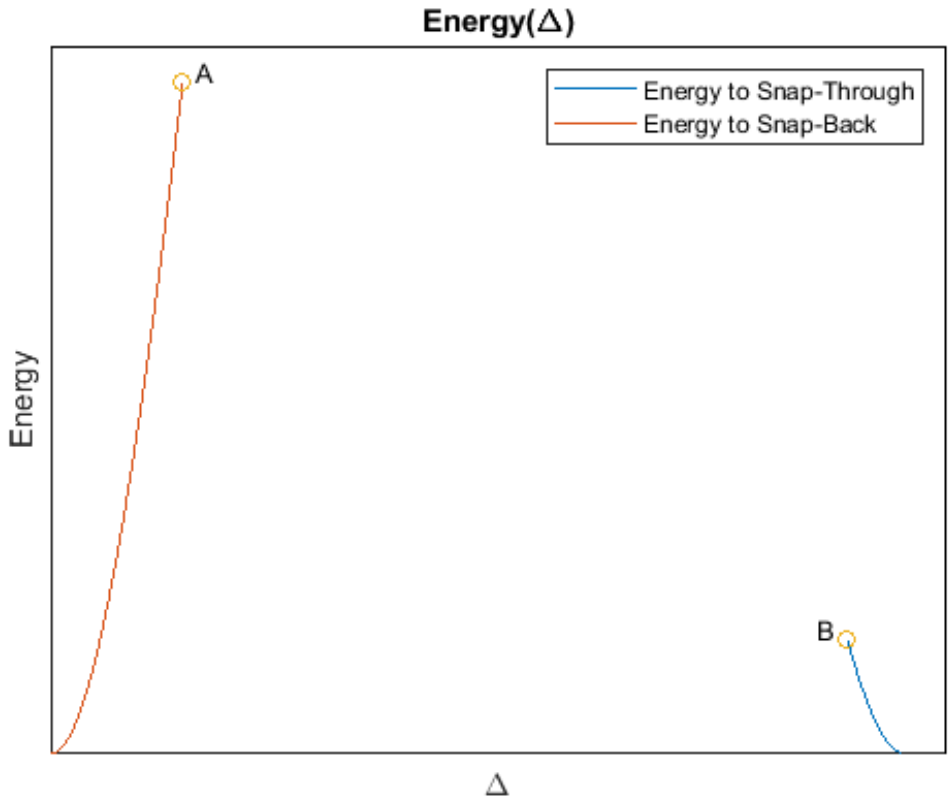

Figure 1.11: Δ-E_{loss}

a business card with two fingers produces an arc. When pressing down on the apex of this arc, energy is inserted to the system. Once the card has passed a critical threshold, the card snaps-through under its own volition. Once snap-through begins, it isn't touching the finger anymore and it moves on its own. Because the card isn't touching the finger anymore, the finger can't apply any force to the card. Meaning there is no energy being inserted to the system. This causes a sudden stop of energy insertion occurring at point A in figure 1.11. The same happens in the reverse; with a person applying force in the opposite direction until the card snaps back; and again the finger leaves the card.

This business card analogy can be seen better in figure 1.12. Starting at the top, row A shows the business card prior to loading. Once the finger comes in contact with

the card, seen in row B, the card begins to deform, and the force-displacement curve begins to progress. Once the loading has reached a certain point, snap-through begins. In figure 1.12 this is seen in row C. The sudden decrease in the force-displacement curve is the result of the finger no longer in contact with the card; meaning the force being applied to it is zero. Row D shows the snap-through position of the card, as well as the complete force-displacement curve. The complete force-displacement curve seen in D forms a triangle-like shape. The area of this triangle directly relates to the total energy being inserted into the system.

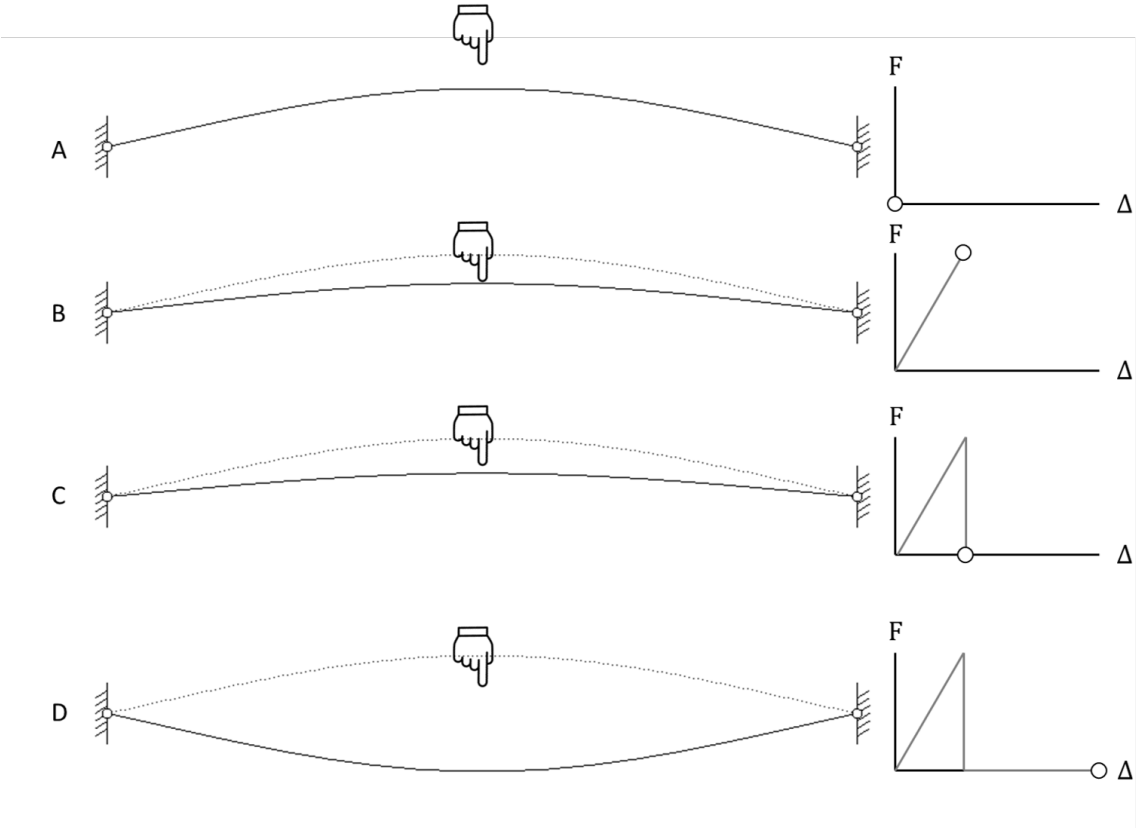

Figure 1.12: Business Card Analogy

This analogy provides a good example of how the bistable curved beam mechanism works, however, there are a few differences between the business card and the curved-bistable system. To begin with: business cards are flat. By flexing the card into the shape of the curved beam, one is stressing the structure. In contrast, the bistable

curved beams are pre-manufactured in their curved state. The other difference is in the boundary conditions; squeezing the card with two fingers applies a roller-roller boundary condition, compared to the fixed-fixed boundary condition found in the curved-beam structure. A system with the same features of the business card has been investigated previously and has a perfectly symmetric force-displacement curve [1]. If the force-displacement curve is symmetric, this means the areas contained to snap-through and snap-back are the same; ie there is no energy loss in this structure. This is yet another reason why the curved bistable beam is needed.

Moving back to the literature, an equation for maximum stress is provided in [6] and can be seen in equation 1.14. This equation can be used to find the maximum stress of the system and ensure the system does not yield.

$$\sigma_{max} = \pi^2 \frac{Eht}{l^2} \left(\frac{4}{3} + \frac{4}{3Q} + \frac{4}{27} \sqrt{\frac{192}{\pi^2} + 162 - 972 \frac{1}{Q^2}} \right) \tag{1.14}$$

Lastly, the ratio $h : t$ must be constrained above a 2.314 value or the system itself will not exhibit bistablility [9]. This makes one of the constraints to be equation 1.15.

$$\frac{h}{t} > 2.314 \tag{1.15}$$

1.2.3 Network of Beams

Up to this point, only a single bistable beam has been discussed. However, the goal of this research is to produce a metamaterial or metastructure out of multiple bistable beams. These beams can be combined in several ways to produce a mesh of beams. [2] studied a rectangular mesh pattern as seen in figure 1.13.

The mesh seen in figure 1.13 features uniform beams and therefore it could be as-

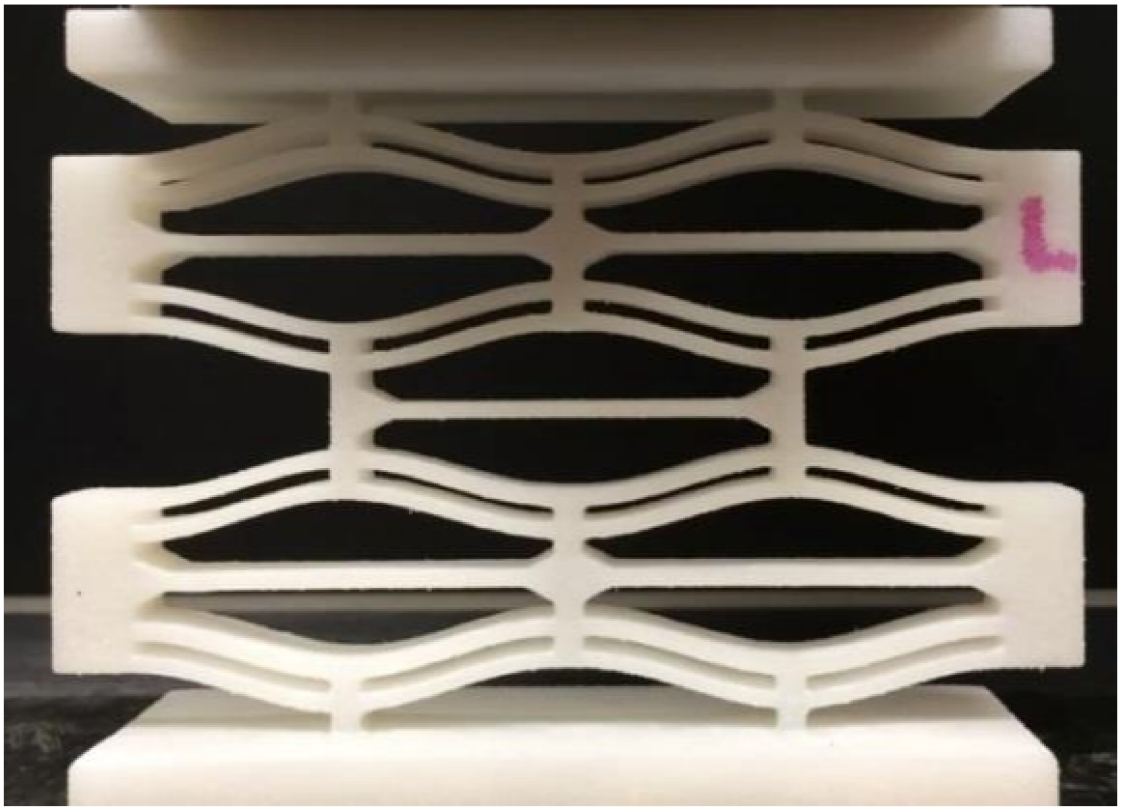

Figure 1.13: Rectangular Mesh [2]

sumed that each beam could snap-through at the same time. However, as seen in its corresponding force-displacement curve, figure 1.14, this is not the case. The reason for this difference is minor perturbations in the powder that makes up the structure [2]. These minor changes cause each beam to vary very slightly, which causes each beam to buckle at different displacements.

This structure was produced out of nylon 11. When loaded from the top, the structure produced the force-displacement curve seen in figure 1.14. The top curve of figure 1.14 is the loading path the force-displacement curve takes, while the lower curve is the unloading portion. Just like the force-displacement curve of a single beam, the loading and unloading paths are different in the mesh structure. The difference between the two curves is the energy lost by the system.

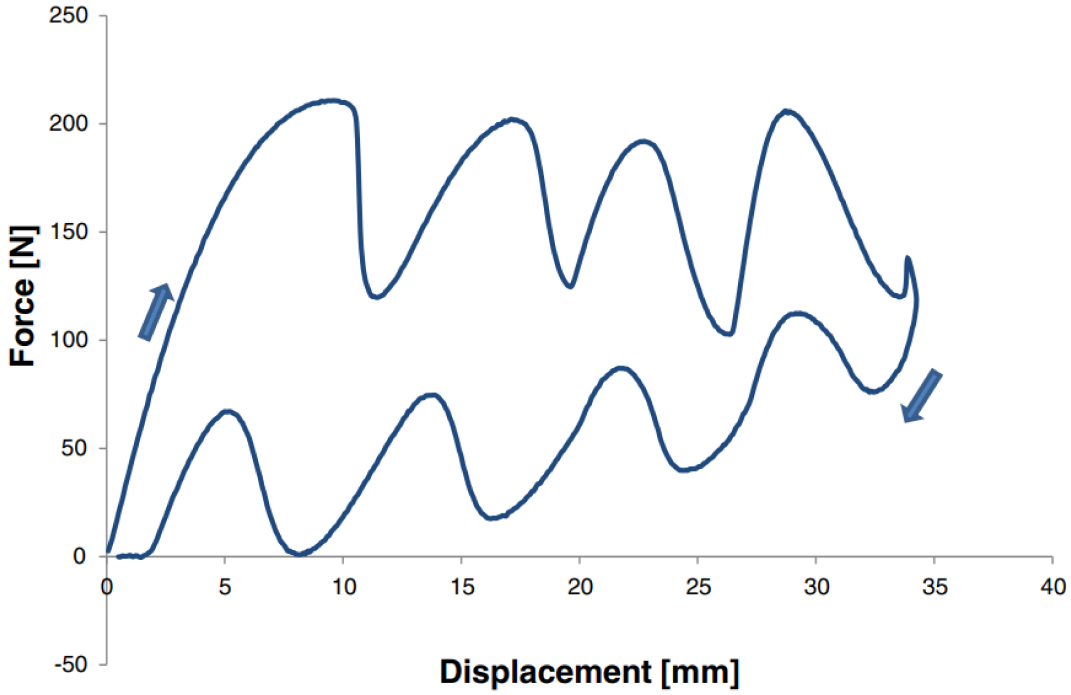

Figure 1.14: Force-Displacement curve of Rectangular Mesh [2]

The top curve of figure 1.14 features several "hills" that bear resemblance to a single beam's snap-through behavior as seen in figure 1.10. These peaks correspond to each individual beam snapping-through [2]. To obtain the total area underneath the top curve in figure 1.14 simply add each individual beam's area together, ie:

$$E_{loading} = \sum E_{loading for Single beam} \tag{1.16}$$

A similar reasoning can be applied to the lower curve.

$$E_{unloading} = \sum E_{unloading for Single beam} \tag{1.17}$$

As seen in figure 1.13, there are horizontal supports that run the span of these cells. These supports exist to prevent expansion and rotation of the cell during loading [2]. If the expansion and rotation were not suppressed, the boundary conditions found in

equation 1.4 would not be enforced. These changes limit the stiffness behavior of the structure [2].

Chapter 2

Energy loss and Force-Displacement Curve Investigation

2.1 Derivation of Energy Loss

The force-displacement curve of the structure alongside mode 2 and 3 buckling can be seen in figure 1.9. If mode 2 buckling is suppressed, figure 1.9 becomes figure 2.1. Figure 2.1 features both the loading curve (equation 1.9) and mode 3 buckling (equation 1.11).

Once the loading path (solid line) intersects the buckling mode, the loading path shifts away from its current loading path. Figure 2.1 shows that there are two intersections along the loading path. At those locations, snap-through is either beginning or ending. Figure 2.2 shows the loading curve with these transition points circled.

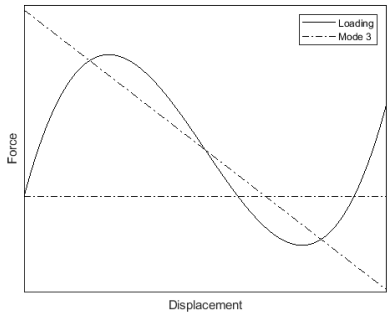

Figure 2.1: Force Displacement Curve with Buckling Modes 3

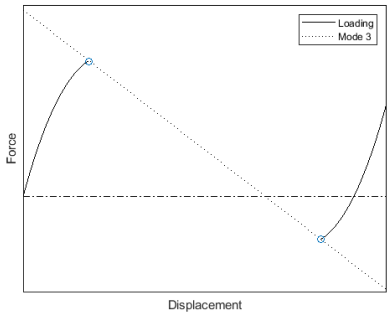

Figure 2.2: Force Displacement Curve with Buckling Mode Hidden

As mentioned in Section 1.3, these two transition points are not directly connected as seen in figure 1.10 under force-controlled situations. Rather, as soon as the system receives enough loading to begin snap-through, the resulting force into the system is reduced to zero. This is because the system no longer needs any additional force for displacement to occur, and the system buckles under its own volition. With this in mind, the true force-displacement curve of the system can be seen in figure 2.3.

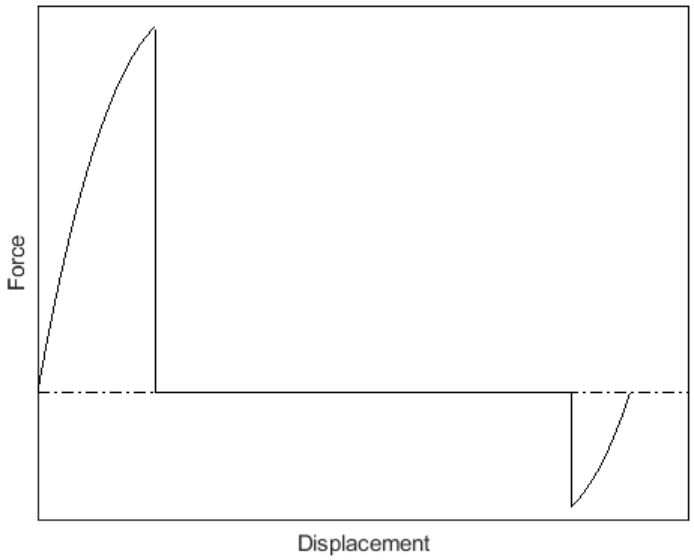

Figure 2.3: True Force Displacement Curve

From figure 2.3, the force-displacement curve produces two clear areas each relating to loading or unloading. Figure 2.4 highlights these areas so they may be discussed

easier. Area A represents the total energy added to the system to cause snap-through. Area B represents how much energy is necessary to snap-back. The reason for it lying under the curve is that the force required to return the system to its first stable point is in the opposite direction of the force required to deform the system.

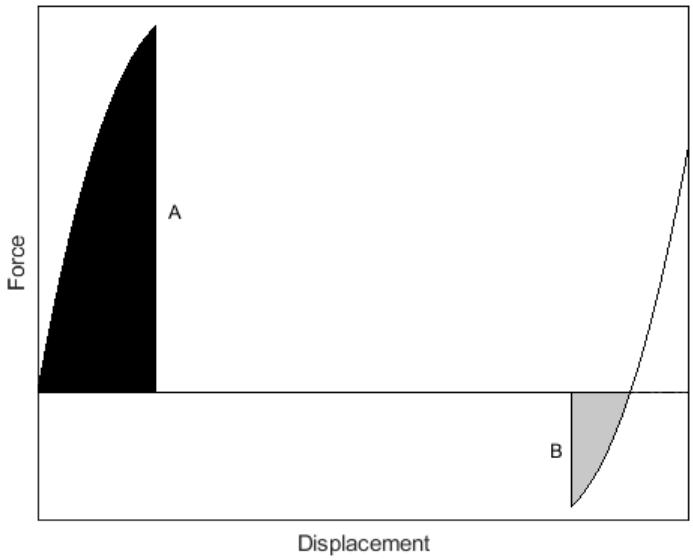

Figure 2.4: Force Displacement Curve with Highlighted Areas

A quick glance at figure 2.4 shows these two areas are not the same, with the purple area being larger than the orange area. Calculating the difference in the areas can be obtained by integrating across both sections, and subtract the unloading area from the loading area. i.e.:

$$E_{loss} = Area_A - Area_B = E_{loading} - E_{unloading} \tag{2.1}$$

2.2 Example Energy Loss Calculation

Take a beam with the following dimensions:

$$h = 6\text{mm}$$

$$t = 0.75\text{mm}$$

$$l = 150\text{mm}$$

$$E = 113.8E3\text{MPa}$$

$$b = 10\text{mm}$$

Running a simulation with displacement control yields figure 2.5. The corresponding force-controlled curve is seen in figure 2.6.

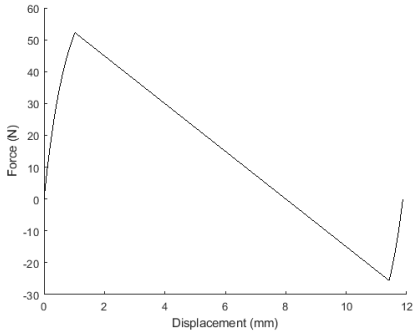

Figure 2.5: Resulting Force-Displacement Curve

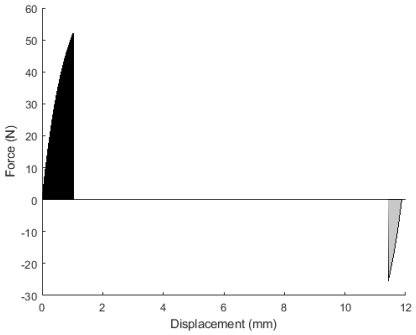

Figure 2.6: Highlighted Areas

Trapezoidal integration on these areas yields:

$$E_{loading} = 32.6229\text{mJ} \tag{2.2}$$

$$E_{unloading} = 6.4685\text{mJ} \tag{2.3}$$

Using the results from 2.2 in equation 2.1 yields the energy lost by the structure:

$$E_{loss} = 26.1544\text{mJ}$$

2.3 Conclusion

With the knowledge of how the energy is lost by a single spring via equation 2.1, investigation can begin on how the assembly of the system will behave.

Chapter 3

Investigation of System Behavior

3.1 System Level Introduction

Moving beyond a single beam, there are two main ways to assemble snap-through beams to attempt to maximize energy loss and creating a suspension system. They can either be assembled in a rectangular or triangular mesh as seen below:

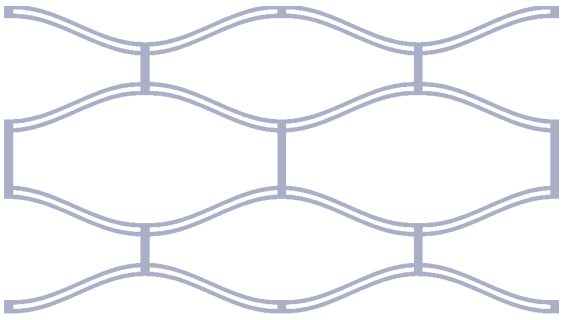

Figure 3.1: Rectangular Mesh

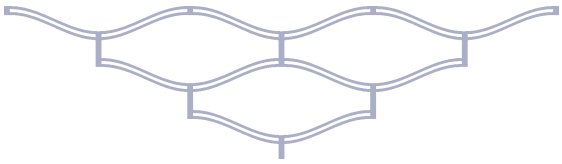

Figure 3.2: Triangular Mesh

[2] puts horizontal supports in these cells as seen in figure 1.13. These horizontal supports are vital, as they enforce the boundary conditions found in equation 1.4. During loading without these horizontal supports, the beams would deflect outward, affecting the bistable and snap-through behaviors. This document assumes that the

boundary conditions found in equation 1.4 are enforced. They can be enforced by either the horizontal beams as seen in figure 1.13, or by the usage of rollers attached to the vertical connectors. During loading, the outside edges of the structure flex outward. It will be assumed that this movement is constrained.

Regardless of which assembly is chosen, each has energy loss associated with it. There are, however, nuances between the two arrangements when it comes to the deformation pattern, the exact calculation of energy loss, and the stress generated within the structure. This chapter discusses and derives these differences.

3.2 Energy Loss at the System Level

To sum the energy lost by the overall system consisting of several smaller cells, one sums the energy lost by each individual cell:

$$E_{systemloss} = \sum_{j}^{n} \sum_{i}^{m} E_{loss_{i,j}} \tag{3.1}$$

where i and j relate to the row and column the cell lies on respectively. The $E_{loss_{i,j}}$ would be calculated as it was previously shown in equation 2.1 with any dimensional changes specific to that beam.

When it relates to each of the meshes, equation 3.1 can be simplified with a few assumptions. For the rectangular case, if the cells only vary row to row, and not column to column, 3.1 simplifies down to:

$$E_{Rectangularsystemloss} = \sum_{j}^{n} n \times E_{loss_j} \tag{3.2}$$

Similarly, the triangular mesh becomes:

$$E_{Triangularsystemloss} = \sum_{j}^{n} j \times E_{loss_j} \tag{3.3}$$

Because the dimensions are changing throughout the structure, equations 3.2 and 3.3 can be used for metastructures. Periodic-metamaterials feature a single cell replicated throughout a mesh and a cell size much smaller than the design domain. If the cells do not change throughout the mesh, the energy loss for a rectangular periodic-metamaterial becomes:

$$E_{UniformRectangularsystemloss} = E_{loss} \times n \times m \tag{3.4}$$

Likewise, the periodic-metamaterial's E_{loss} for a triangular mesh becomes:

$$E_{UniformTriangularsystemloss} = \frac{1}{2} E_{loss} \times n(n+1) \tag{3.5}$$

3.3 Stresses Generated in Vertical Connectors

3.3.1 Introduction

The meshes consist of several beams attached to one another. As seen in either figures 3.1 or 3.2, there are vertical connectors that attach each beam together. These connections are "legs" that the beams stand on to form a mesh. Seeing how the maximum stress within the curved beam portions are known by equation 1.14, the connecting regions are the only regions in which the stress is not known. If the stress is determined in these regions, the stresses throughout the structure will be known and can be designed to not surpass its yield limit.

As mentioned in the introduction of this chapter, it will be assumed that the beam's ends are held in such a way to enforce the boundary conditions found in 1.4. Additionally, the legs will be considered thick enough as to not buckle.

3.3.2 Rectangular Mesh

To get a free body diagram of the system, one can simplify the curved-beam system shown previously in figure 1.2. Simplifying this drawing to a stick drawing yields:

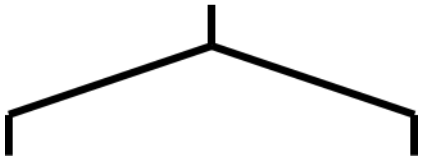

Figure 3.3: Single Cell

Using figure 3.3 along with figure 3.1 one can create a simplified stick drawing of the rectangular system seen in figure 3.4.

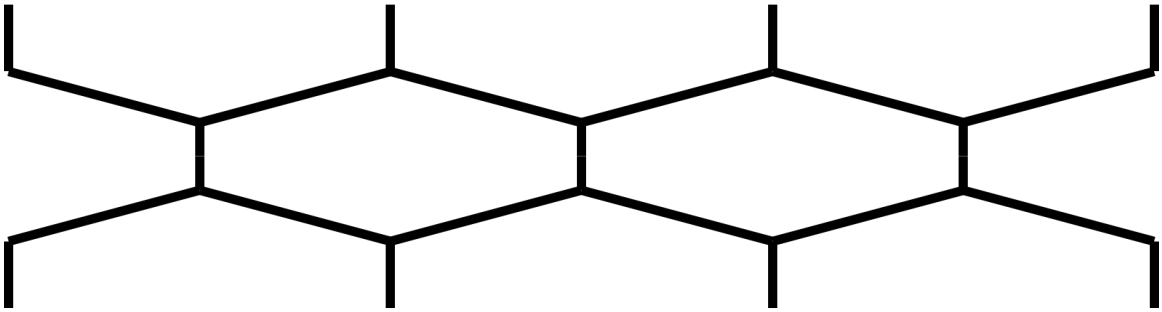

Figure 3.4: Stick Rectangular Mesh

Focusing on a single row; setting a force F distributed on the top of the structure and fixing the bottom yields the free-body diagram seen in figure 3.5

Figure 3.5 shows that the forces within the structure remain the same, while the forces on the outside are half-that of the inside. Generalizing the rectangular mesh seen in

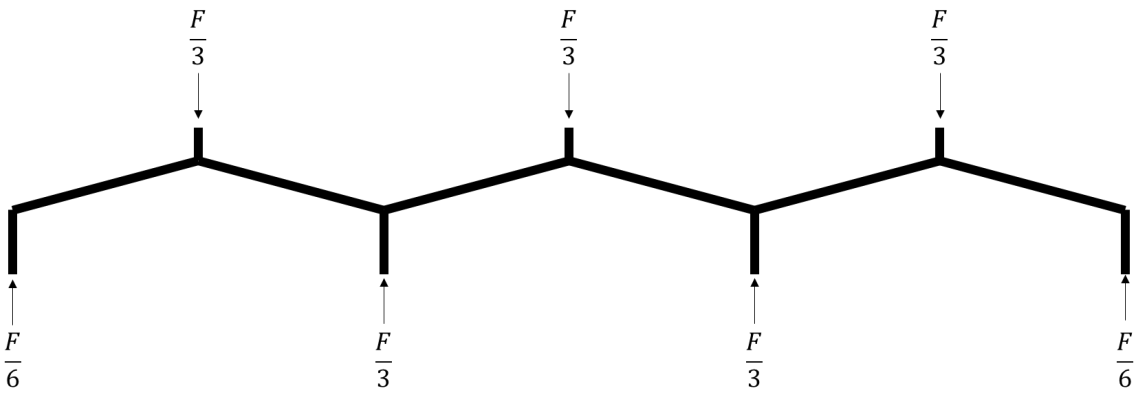

Figure 3.5: Rectangular Free Body Diagram

figure 3.5 to all rectangular meshes yields:

$$f_{internalbeam} = \frac{f_{applied}}{m} \tag{3.6}$$

$$f_{externalbeam} = \frac{1}{2} f_{internalbeam} = \frac{1}{2} \frac{f_{applied}}{m} \tag{3.7}$$

where m is the number of beams in a row

Assuming the legs are thick enough to prevent any buckling; the moment being applied to the tip of each leg is:

$$m_{externalbeam} = \frac{1}{4} \frac{f_{applied}}{m} L \tag{3.8}$$

This moment is only present on the outside beams as internal beams produce couples that cancel one-another out.

Putting everything together, the normal stress for the internal member's legs are:

$$\sigma_{Rectangularinternal} = \frac{F}{A} = \frac{f}{xt_2 b} \tag{3.9}$$

where t_2 is the thickness of the supporting leg as seen in figure 3.6

The external beams have combined loading from the resulting normal stress from the

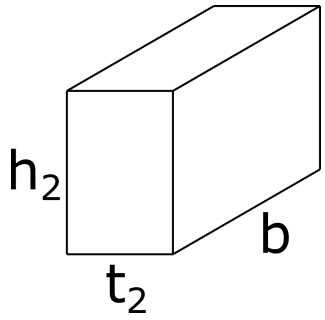

Figure 3.6: Connector Variables

axial force and the normal stress generated by the resulting moment. When combined, the stress for the external beams are:

$$\sigma_{RectangularExternal} = \frac{F}{A} + \frac{My}{I} = \frac{f}{2xt_2b} + \frac{3fL}{2xbh_2^3} \tag{3.10}$$

where h_2 is the height offset between the beams, t_2 is the thickness of each leg, and I is the moment of inertia

3.3.3 Triangular Mesh

Using the stick drawing found in figure 3.3 and the reference from 3.2 a stick drawing of the triangular mesh can again be constructed. This stick drawing can be seen in figure 3.7.

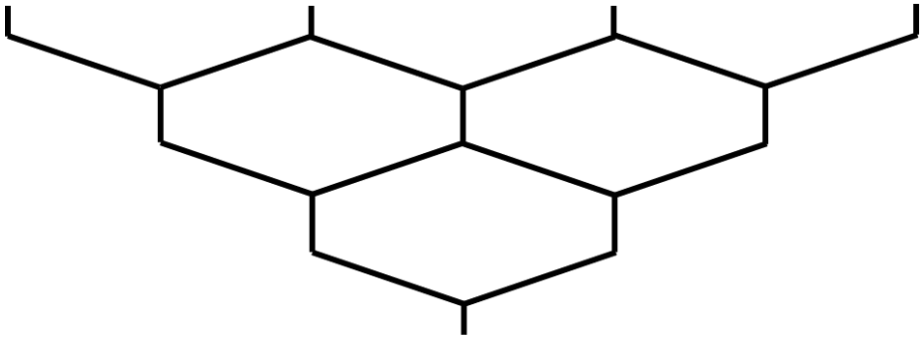

Figure 3.7: Stick Triangular Diagram

Just like the rectangular mesh, this can be solved statically. Doing so yields figure 3.8.

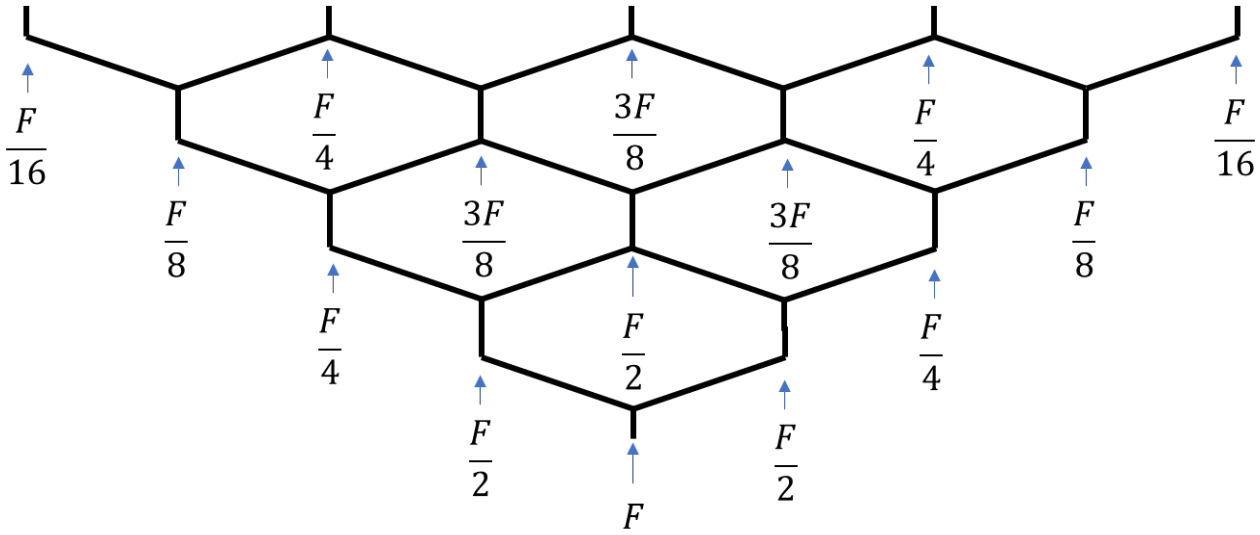

Figure 3.8: Triangular Free body Diagram

While one could use the force being applied on each individual leg to find the dimensions of that leg, this would result in varying t_2, causing beam spans to change slightly throughout a row; causing meshing problems between layers. Designing each row's leg to withstand the maximum force being applied to that row, ensures that meshing problems stemming from varying beam spans do not occur.

Figure 3.8 shows that the forces in each row are at a maximum in the center of the structure. Each rows maximum force is given by:

$$F_{maxtriangular} = F\binom{K}{\frac{K}{2}} \times \frac{1}{2^K} \begin{cases} K = n & \text{when } n \text{ is even} \\ K = n+1 & \text{when } n \text{ is odd} \end{cases} \tag{3.11}$$

Knowing this, each row's leg should be designed to support:

$$\sigma_{Triangular} = \frac{F_{maxtriangular}}{t_2 b} \tag{3.12}$$

3.3.4 Redimensionalizing F

Equations 3.9, 3.10, and 3.12, are functions of the input force. Seen in figure 2.3, the maximum force applied to the structure occurs right as snap-through begins. Snap-through is a geometric phenomenon that occurs at a known displacement. [6] approximates this displacement as:

$$d_{maxForce} = h\left(\frac{28}{27} - \pi\frac{2}{3}\sqrt{\frac{1}{6} + \frac{16}{81\pi^2} - \frac{1}{Q^2}}\right) \tag{3.13}$$

While there is no equation for the force-displacement curve with higher buckling modes; snap-through occurs when $N = 4\pi$ [6]. Knowing this, and then combining it with equations 3.13 and 1.13 yields the maximum force necessary for snap-through:

$$f_{max} = \frac{1}{12}\frac{Ebht^3}{l^3}\left(\frac{512}{27}\pi^2 + \pi^3\frac{128}{3}\sqrt{\frac{1}{6} + \frac{16}{81}\pi^2 - \frac{1}{Q^2}}\right) \tag{3.14}$$

Using this equation, f can now be substituted in equations 3.9, 3.10, and 3.12. Doing so yields:

$$\sigma_{RectangularInternal} = \frac{1}{12}\frac{Ebht^3}{l^3}\frac{\pi^2}{xt_2b}\left(\frac{512}{27} + \pi\frac{128}{3}\sqrt{\frac{1}{6} + \frac{16}{81}\pi^2 - \frac{1}{Q^2}}\right) \tag{3.15}$$

$$\sigma_{RectangularExternal} = \frac{1}{12}\frac{Ebht^3}{l^3}\frac{\pi^2}{2xb}\left(\frac{1}{t_2} + \frac{3lt_2}{h_2^3}\right)\left(\frac{512}{27} + \pi\frac{128}{3}\sqrt{\frac{1}{6} + \frac{16}{81}\pi^2 - \frac{1}{Q^2}}\right) \tag{3.16}$$

$$\sigma_{TriangularExternal} = \frac{1}{12}\frac{Ebht^3}{l^3}\frac{\pi^2}{t_2b}\left(\frac{512}{27} + \pi\frac{128}{3}\sqrt{\frac{1}{6} + \frac{16}{81}\pi^2 - \frac{1}{Q^2}}\right) \times \binom{K}{\frac{K}{2}}\frac{1}{2^K} \tag{3.17}$$

In the event that uniform leg dimensions throughout the structure are required, equations 3.15, 3.16 and 3.17 can be altered to become:

$$\sigma_{RectangularInternal} = \frac{1}{12} E C_1 \frac{\pi^2}{x t_2} \left(\frac{512}{27} + \pi \frac{128}{3} \sqrt{\frac{1}{6} + \frac{16}{81}\pi^2 - C_2^2} \right) \tag{3.18}$$

$$\sigma_{RectangularExternal} = \frac{1}{12} E C_1 \frac{\pi^2}{2x} \left(\frac{1}{t_2} + \frac{3 l t_2}{h_2^3} \right) \left(\frac{512}{27} + \pi \frac{128}{3} \sqrt{\frac{1}{6} + \frac{16}{81}\pi^2 - C_2^2} \right) \tag{3.19}$$

$$\sigma_{TriangularExternal} = \frac{1}{12} E C_1 \frac{\pi^2}{t_2} \left(\frac{512}{27} + \pi \frac{128}{3} \sqrt{\frac{1}{6} + \frac{16}{81}\pi^2 - C_2^2} \right) \times \binom{K}{\frac{K}{2}} \frac{1}{2^K} \tag{3.20}$$

where C is:

$$C = max \left\{ \frac{h_c t_c^3}{l_c^3}, \frac{t_c}{h_c} \right\} \tag{3.21}$$

where c is every beam

It is likely that only h and t would vary in between beams, with l being defined by the problem statement. If that were the case, l could be held constant in equation 3.21.

3.4 Deformation Pattern

If the cells change from row to row, each row will snap at alternative displacements. This section will show when these transactions occur, and how to predict and utilize them.

3.4.1 Introduction

As seen in figures 3.1 and 3.2, each system consists of multiple rows of curved beams. Figure 1.14 shows that near uniform beams buckle at different displacements. The reason that some beams buckle before others is a result of minor perturbations during manufacturing that effects that beam's stiffness. Less stiff beams reach the force necessary to snap-through before more stiffer beams. On the system level, the force felt by each beam is the same. Because the force to cause the less stiff beams is less than the stiffer beams, they snap-through first. This indicates that the system will snap-through in ascending order of beam stiffness. If the stiffness of each beam can be uncovered, the beams can then be sorted accordingly. This can cause the system to snap-through bottom-up, top-down, or a mix of the two.

3.4.2 Derivation

Stiffness is defined as:

$$k = \frac{F}{d} \tag{3.22}$$

Equation 3.22 can be used along side equations 3.13 and 3.14 to calculate the stiffness of a single curved beam. As the exact stiffness is not required, the constants will be ignored to create a simpler equation. The simplified stiffness equation can be seen in 3.23.

$$k \cong \frac{Ebt^3}{l^3} \tag{3.23}$$

To reiterate, in this instance, it is desired that the beams deform in a specific order. Under most circumstances, the depth of the beam, b, the span of the beam, l, and the material it's made out of will remain constant throughout the structure. This leaves t as the only variable. To differentiate between rows, the subscript n can be used,

where n is the nth row starting from the bottom row; row 0.

With these in mind, the stiffness of the initial row can be related to the stiffness of the nth row. Thus, relation 3.23 yields:

$$t_0^3 :: t_n^3 \tag{3.24}$$

Dropping the cube root and dividing the LHS by the RHS produces:

$$\frac{t_0}{t_n} :: 1 \tag{3.25}$$

If the initial beam is stiffer than the nth beam, that means that the nth row will buckle before the initial row, meaning if:

$$\frac{t_0}{t_n} > 1 \tag{3.26}$$

The system would buckle in descending order (top-down). Likewise, if:

$$\frac{t_0}{t_n} < 1 \tag{3.27}$$

The nth row would buckle before the initial row. So, the system would buckle in ascending order (bottom-up). The final arrangement is:

$$\frac{t_0}{t_n} = 1 \tag{3.28}$$

This would cause each row to buckle at the same time. While this might be interesting, minor perturbations at the manufacturing level prevent this from being realisable as seen in figure 1.14.

Relations 3.26, 3.27, and 3.28 only force the beams to buckle in a specific order,

ascending or descendingly. If finer control is required, multiplying a stiffness-factor, f_n, would result in each beam being f times smaller or larger from the initial beam. Doing this to equation 3.25 results in:

$$t_0 :: f_n t_n \tag{3.29}$$

f_n can remain constant to give a uniform stiffness scaling throughout the structure. Alternatively, f_n could be altered between layers to give a non-uniform stiffness scaling. More interestingly f_n could fluctuate being above and below 1, to make beams deform in a unique pattern, or be optimized to fit a specific pattern.

3.4.3 FEA Deformation Example

To validate the results obtained from the deformation analysis, n FEA model was created to test the deformation pattern.

Using Abaqus, a 2D dynamic-implicit model was created. Made from Titanium the following variables were used: $E = 113.8E3$, $\nu = 0.35$ and $l = 100$ were used throughout the structure. To get a specific deformation pattern, relation 3.26 was used. The dimensions of each beam can be seen in table 3.1. The initial mesh alongside the

		h	t
beam (top-down)	0	5	1
	1	4	0.75
	2	5	0.5
	3	6.33	0.25

Table 3.1: Curved Beam dimensions 0-3

boundary conditions can be seen in figure 3.9. This also shows the curved beams and their numbers associated with table 3.1.

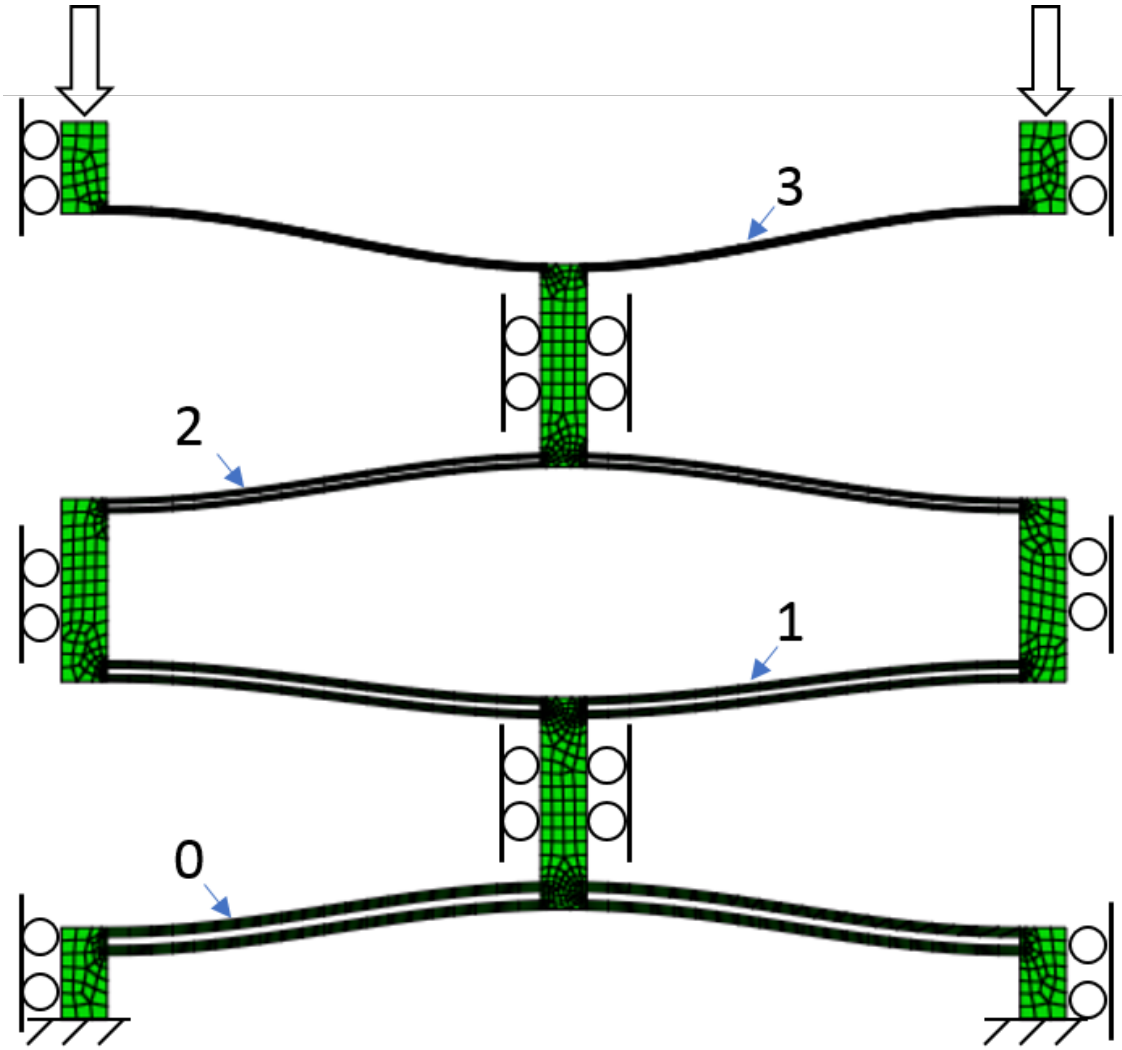

Figure 3.9: Initial FEA model with BC shown for Deformation Test

The results of the simulation can be seen in figure 3.10. On the left side of figure 3.10 is the initial shape of the structure. Moving left to right indicates the passing of time. The series of images A, B, C, and D show the buckling order the system goes through. This matches the order expected as the beam with the smallest thickness, beam 3, buckles first. This continues in order until the last beam, beam 0, buckles. This order confirms relation 3.24.

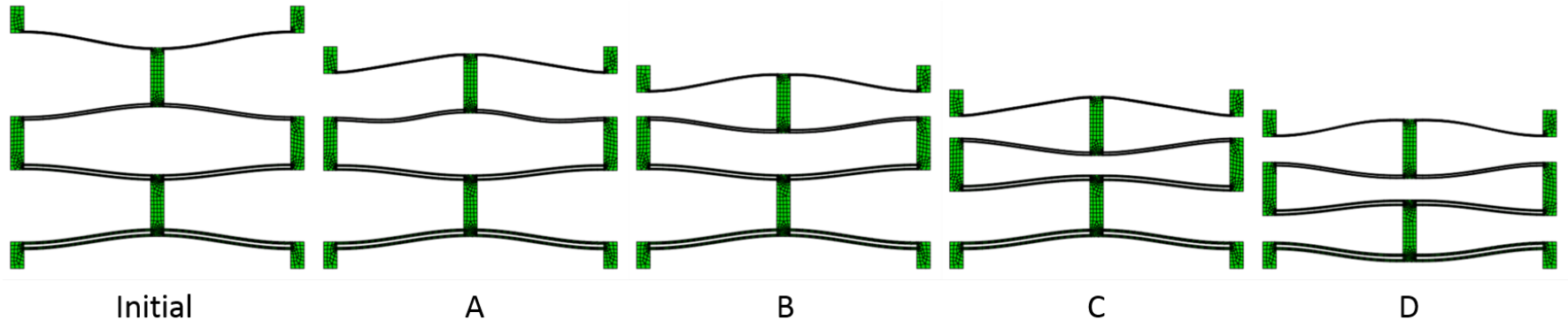

Figure 3.10: FEA Deformation-test Results

3.5 Wrap up

This chapter went over several key components of the metamaterial and metastructure systems. Section 3.2 covers how to calculate the energy lost by the entire system. Section 3.3 discusses the last regions of the system with unknown stress. Lastly, section 3.4 discusses how the beams buckle, and how to control this deformation pattern. With these factors known, investigation now begins on seeing how the system's variables affects E_{loss}.

Chapter 4

Scaling and Surrogate Model

4.1 Introduction

Lacking a direct equation, the amount of energy lost by the structure is obscure. Investigating how the variables E, b, h, t and l affect the energy lost by the system will help to better understand and optimize the structure.

4.2 Scaling Behavior

Geometrically, the variables will not be on the same scale. Broadly speaking:

$$l >> h > t \tag{4.1}$$

One can use this scale to see how the equations of stress and energy scale. Using the scale 4.1 alongside with the curved beam stress equation, equation 1.14, stress

primarily scales with:

$$\sigma_{max} \sim \frac{Eth}{l^2} \tag{4.2}$$

Meaning increasing E, t, or h linearly increases the stress, while l will quadratically decrease it.

E_{loss} does not have a direct equation, so its scale is not as clear. To obtain E_{loss}'s scales, multiple simulations were run to see how variables E, b, h, t, and l effect it. For example, figure 4.1 shows a curve comparing the variable t to the corresponding E_{loss} with a constant E, b, h, and l. Similar graphs for E, b, h, and l are available in Appendix A.

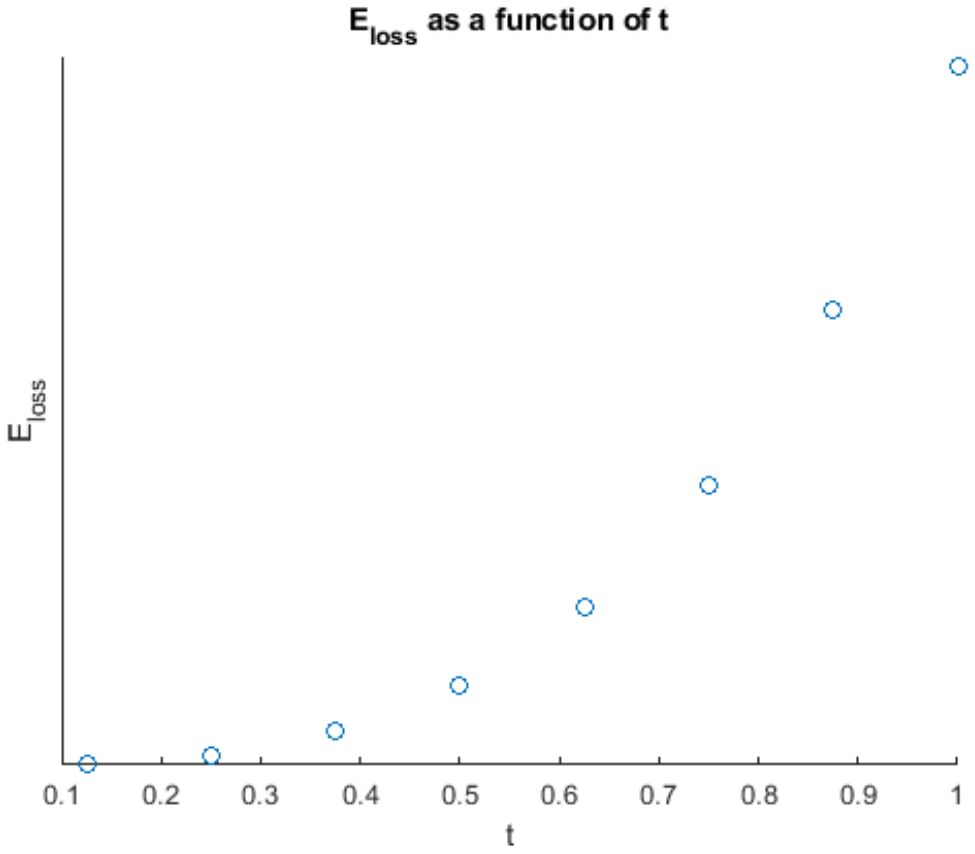

Figure 4.1: E_{loss} as a function of t

Figure 4.1 shows us that t scales the energy cubically. Repeating the process for

variables E, b, h and l,the following scale for energy is produced:

$$E_{loss} \sim \frac{Ebh^2t^3}{l^3} \tag{4.3}$$

Meaning the energy linearly scales with E and b, quadratically with h, and cubically with t; while decreasing cubically with l.

While scales do not tell exactly how much energy is lost, they are helpful in understanding how the structure behaves. To better understand how energy loss is scaled, equation 4.3 may be altered slightly. E and b are likely both defined by the problem, so they may be ignored. Secondly, one can multiply the scale by 1 in the form of t^2/t^2. Doing these, and rearranging the equation, the following is produced:

$$E_{loss} \sim \left(\frac{h}{t}\right)^2 \left(\frac{t}{l}\right)^3 t^2 \tag{4.4}$$

t^2/t^2 was multiplied in to show how the aspect ratios increase the energy loss. With h/t being the height aspect ratio, and l/t being its length aspect ratio. Moving forward the height aspect ratio ${}^h/_t$ will be called Q, while the length aspect ratio ${}^l/_t$ will be called R. Q already has significance [9][6], while the term R was selected to produce a length aspect ratio. The length aspect ratio was selected due to its importance in studying beams. Additionally, scale 4.3 was expanded as testing several dimensions with it gave inconsistent results, hinting at the presence of a coupling term.

A variable can be considered coupled when changing the variable relative to an equa-

tion produces different results. Take two systems with the following variables:

$$E = 1 \qquad E = 1$$
$$b = 1 \qquad b = 1$$
$$h = 6 \qquad h = 2.921$$
$$t = 1 \qquad t = 0.75$$
$$l = 100 \qquad l = 100$$

Using the scale 4.4 produces:

$$EbQ^2R^{-3}t^2 = 3.6\text{E}^{-}5 \qquad EbQ^2R^{-3t}t^2 = 3.6\text{E}^{-}5$$
$$Q = 6 \qquad Q = 3.9$$
$$R = 100 \qquad R = 133.3$$

Because the scales are identical, it would be expected that the E_{loss} would be of the same scale. However, this is not the case, with the right equation giving $E_{loss} = 2.0929\text{E}^{-4}$mJ and the left equation giving $E_{loss} = 2.9757\text{E}^{-5}$mJ. This difference shows the existence of a coupling term. Running multiple simulations varying only Q or R can be seen in figures 4.2 and 4.3. The non-constant behavior of Q shows that it is a coupling term.

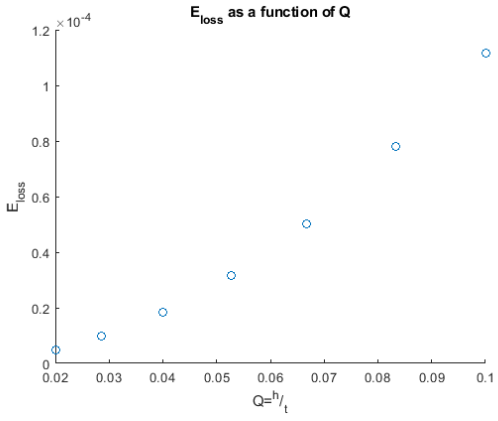

Figure 4.2: E_{loss} as a function of Q

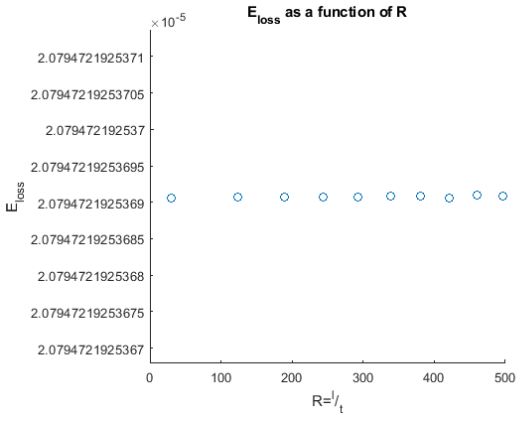

Figure 4.3: E_{loss} as a function of R

Redefining scale 4.4 to use Q and R produces equation 4.5.

$$E_{loss} \sim \ EbQ^2 \frac{1}{R^3} t^2 \tag{4.5}$$

4.3 System Energy Scaling

Say there is a rectangular domain and it is desired to subdivide this domain into a mesh as seen in figure 4.4. What thickness t is required to keep the same E_{loss} scale?

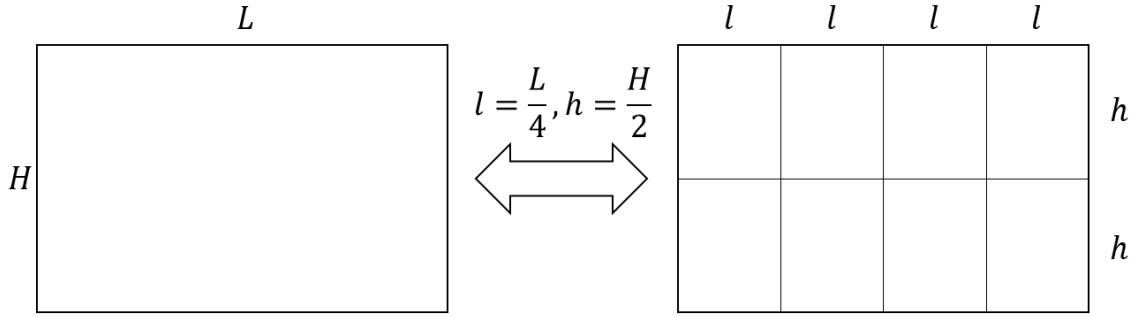

Figure 4.4: Rectangular Scaling Example

The height and length of the system are defined, with the mesh's local height and length defined by:

$$h = \frac{H_0}{n} \tag{4.6}$$

$$l = \frac{L_0}{m} \tag{4.7}$$

where h and l are the height and length of a single curved beam, and H_0 and L_0 are the maximum dimensions of the rectangular mesh.

Defining α to be the thickness scaling coefficient. Using scale 4.4 with equations 4.6 and 4.7 produces:

$$\left(\frac{H_0}{t}\right)^2\left(\frac{t}{L_0}\right)^3 t^2 = n \times m \times \left(\frac{\frac{1}{n}H_0}{\alpha t}\right)^2\left(\frac{\alpha t}{\frac{1}{m}L_0}\right)^3 (\alpha t)^2 \tag{4.8}$$

where the left side is a single curved beam, and the right side is the mesh

Working out equation 4.8, α is found to be:

$$\alpha = \sqrt[3]{\frac{n}{m^4}} \tag{4.9}$$

Equation 4.9 shows us an interesting relation. Given a fixed rectangular domain; subdividing it into additional rows makes each beam's thickness needs to get thicker and thicker just to provide the same energy loss scale. Counter to this, as more columns get added, the thinner the beam's thickness needs to become to match the same energy loss scale. When optimizing the structure, it is expected that the system will always move to the minimum number of rows and the maximum number of columns. This is done to give the largest number of springs, with each spring contributing the same scale of energy loss. This, alongside equation 3.1, provides the largest amount of energy lost by the system. However, when designing the system, the system will have to have some number of rows to fulfill the stress constraint given in equation 1.14.

4.4 Material Selection

Material selection is an interesting factor when it comes to E_{loss}. Both equations of stress and energy scale with E. Choosing a material with a large E would return a structure with a large E_{loss}, but also a large σ_{max}. A large σ_{max} raises concerns about material yielding. Because increasing E increases both E_{loss} and σ_{max}, finding the

material with a high E and σ_{yield} ensures that the stress, while high, remains within its yield limit and gives the largest possible E_{loss}.

4.5 Surrogate Model

A surrogate model is a method used to predict the outcome of an experiment by producing a model that has been fit to match experimental data. To better understand how the variables affect energy loss, a surrogate model will be produced that accurately predicts the energy lost by the system.

It will be assumed that the surrogate model takes the form of equation 4.10.

$$E_{loss} = A(E, b, h, t, l)^{\alpha} \times B(E, b, h, t, l)^{\beta} \times C(E, b, h, t, l)^{\gamma} ... \tag{4.10}$$

The initial scale for E_{loss}, scale 4.3, can be used as one of the functions, leading to equation 4.11.

$$E_{loss} = E \times b \times h^2 \times t^3 \times \frac{1}{l^3} \times B(E, b, h, t, l)^{\beta} \times C(E, b, h, t, l)^{\gamma} ... \tag{4.11}$$

Expanding scale 4.3 into scale 4.4 shows some coupling terms, Q and R. It will be assumed that these two scales make up the functions B and C. With this in mind, equation 4.11 now becomes 4.12.

$$E_{loss} = E \times b \times h^2 \times t^3 \times \frac{1}{l^3} \times B(Q)^{\beta} \times C(R)^{\gamma} \tag{4.12}$$

To produce the surrogate model, the goal is to find these functions of B and C. Figure

4.3 shows the R has no impact on E_{loss}, so its term may be eliminated, leaving only Q. This reduction makes equation 4.12 into equation 4.13.

$$E_{loss} = E \times b \times h^2 \times t^3 \times \frac{1}{l^3} \times B(Q)^{\beta} \tag{4.13}$$

To find the function B, varying Q and keeping the rest of equation 4.13 constant will show some relation between the function of B and E_{loss}. This relation can be seen in figure 4.5 and shows that this relation is linear. Meaning that β in equation 4.13 is equal to 1.

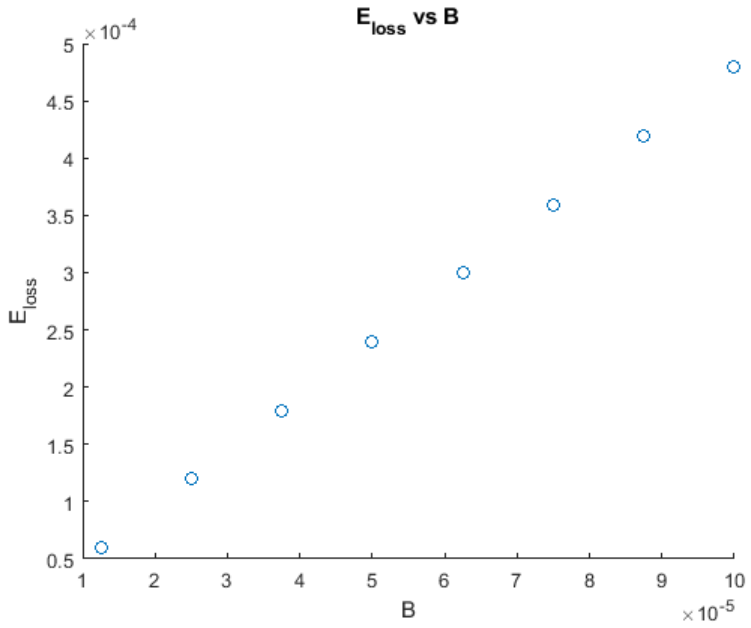

Figure 4.5: Relation between B and E_{loss}

To determine the function of $B(Q)$, equation 4.13 can be rewritten as equation 4.14.

$$B(Q) = \frac{E_{loss}}{\frac{Ebh^2t^3}{l^3}} \tag{4.14}$$

Running multiple simulations produces B as a function of Q. Q was set to a domain of $[3, 30]$. This function is then curve fitted with a rational function of degree 2. This

rational function can be seen in equation 4.15. Equation 4.15 can be seen plotted alongside the experimental data in figure 4.6.

$$B(Q) = \frac{4.251Q^2 + 3.134Q + 45.4}{Q^2 + 0.8436Q - 3.689} \tag{4.15}$$

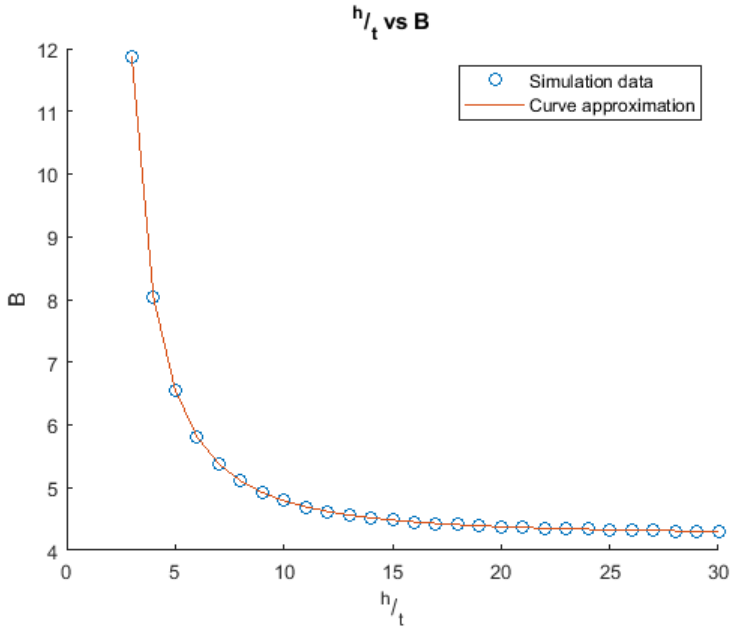

Figure 4.6: B vs $^{h}/_{t}$

A different type of function could have been used in curve fitting, but a rational function gave the best curve fit with an RMS of 1.

Combining equations 4.14 and 4.15 produces equation 4.16 which is the surrogate model of E_{loss}.

$$E_{loss} = Eb\frac{4.251Q^2 + 3.134Q + 45.4}{Q^2 + 0.8436Q - 3.689}\frac{h^2t^3}{l^3} \tag{4.16}$$

A comparison between the surrogate model and the theoretical model can be seen in figure 4.7. The dimensions of each simulation were obtained by using a latin-hyper-cube on the ranges of $Q = [3, 30]$ and $R = [30, 500]$. The exact dimensions used and the results can be seen in Appendix B.

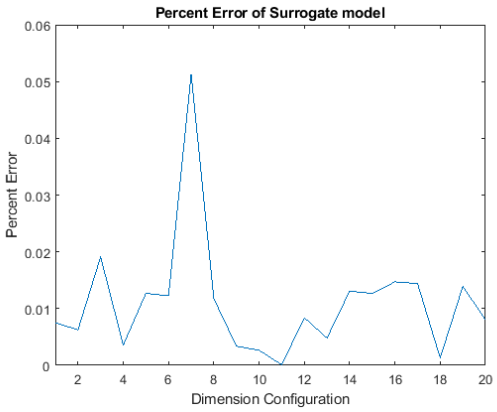

Figure 4.7: Surrogate Model alongside Experimental Data

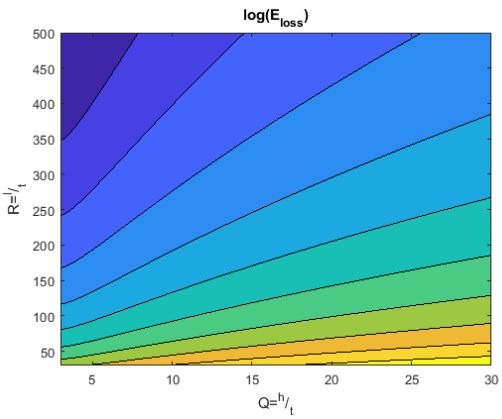

Figure 4.8: Contour plot of E_{loss}

Figure 4.7 shows a strong agreement between the theory and the surrogate model, with the largest percent error being 0.05%. $B(Q)$ was obtained from curve fitting over the range of [3, 30]. For cases in which Q is outside of this range, a new function of $B(Q)$ will have to be curve fitted to approximate the system.

The surrogate model can be used to rapidly predict the energy lost by the system. Using it, a contour plot of E_{loss} can be seen in figure 4.8. It shows that E_{loss} is maximum when the height aspect ratio is maximized, while the length aspect ratio is minimized.

Using the surrogate model alongside equation 1.14 (maximum stress in the curved beam) allows us to see the domain of solutions. Titanium has a Young's Modulus of 113.8GPa and yield stress of 970MPa [7]. Using these as the E and maximum stress values, a contour plot of E_{loss} can be seen in figure 4.9. The highlighted point on the right side is the maximum E_{loss}. The white zone on the bottom-right side is where the stress exceeds the yield limit.

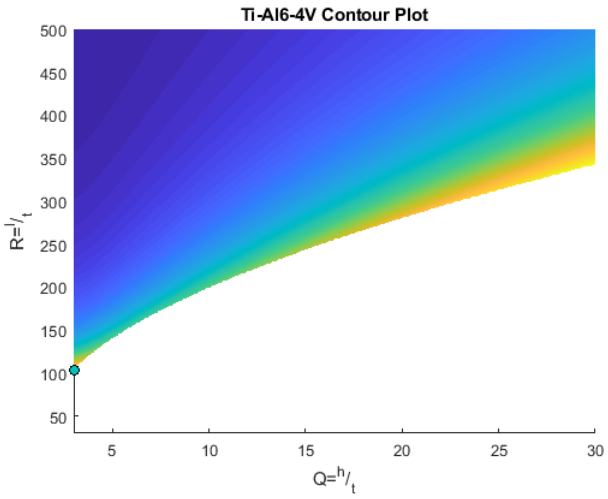

Figure 4.9: Domain of Solutions for Titanium

A similar plot may be produced for AISI 1006 steel, with an $E = 206\text{GPa}$ and $\sigma_{yield} = 285\text{MPa}$ seen in figure 4.10.

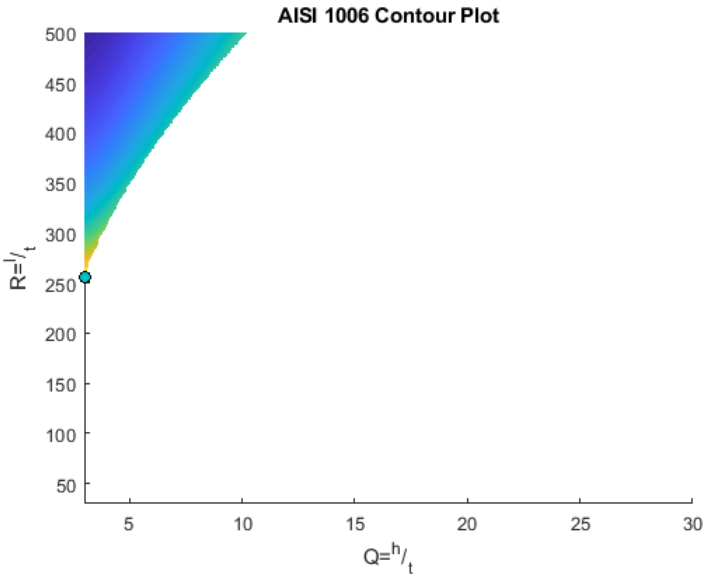

Figure 4.10: Domain of Solutions for AISI 1006

A third contour plot can be seen in figure 4.11 made from a Aluminum 6061-T6 with $E = 68.9\text{GPa}$ and $\sigma_{yield} = 276\text{MPa}$

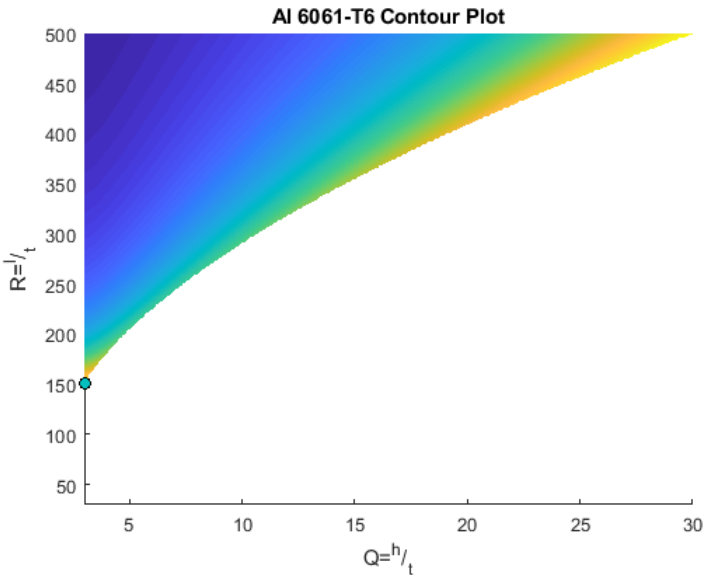

Figure 4.11: Domain of Solutions for Al 6061T6

4.6 Effect of Number of Cells on Energy Loss

A metamaterial consists of a number of uniform cells in multiple directions. Equation 4.16 can be used alongside equations 4.6 and 4.7 to calculate what number of rows and columns provide the most energy loss similar to how the scaling coefficient α was found in equation 4.8.

To compare mesh sizes, it will be assumed that the rectangular domain L_0 wide and H_0 has been found. In it features a single spring spanning those dimensions with a thickness T_0. This single spring will then be compared to a mesh of smaller springs that combined fill the same domain. The mesh of springs consists of $Num.$ springs.

Similar to the local h and l found in equations 4.6 and 4.7, a similar reduction can be made for t.

$$t = \frac{T_0}{n} \tag{4.17}$$

Using equations 4.6, 4.7 and 4.17 in 4.16 produces:

$$\begin{aligned} Eb\frac{4.251Q^2+3.134Q+45.4}{Q^2+0.8436Q-3.689}\frac{H_0^2T_0^3}{L_0^3} &= \text{Num.} \times Eb\frac{4.251Q^2+3.134Q+45.4}{Q^2+0.8436Q-3.689}\frac{\frac{H_0}{n}^2\frac{T_0}{n}^3}{\frac{L_0}{m}^3} \\ \frac{H_0^2T^3}{L_0^3} &= \text{Num.} \times \frac{\frac{H_0}{n}^2\frac{T_0}{n}^3}{\frac{L_0}{m}^3} \\ &= \text{Num.} \times \frac{m^3}{n^5}\frac{H_0^2T_0^3}{L_0^3} \\ 1 &= \text{Num.} \times \frac{m^3}{n^5} \end{aligned} \tag{4.18}$$

If the mesh is uniformly reduced in size, m=n, meaning equation 4.18 becomes:

$$1 = \text{Num.} \times \frac{1}{m^2} \tag{4.19}$$

For a rectangular mesh, Num. is:

$$\text{Num.} = \begin{cases} n \times m \\ m^2 \qquad \text{when uniform} \end{cases} \tag{4.20}$$

Equations 4.19 and 4.20 indicate that reducing the single meta-material spring into similar smaller springs has no impact on energy loss. If the system is not reduced uniformly, equation 4.18 alongside 4.20 becomes:

$$E_{loss} = \frac{m^4}{n^4}Eb\frac{4.251Q^2+3.134Q+45.4}{Q^2+0.8436Q-3.689}\frac{h^2t^3}{l^3} \tag{4.21}$$

A similar approach can be done with triangular meshes, with the number of springs found in them to be:

$$\text{Num.} = \frac{1}{2} \times m(m+1) \tag{4.22}$$

Making the energy lost for a triangular mesh:

$$E_{loss} = \frac{1}{2}m(m+1)Eb\frac{4.251Q^2 + 3.134Q + 45.4}{Q^2 + 0.8436Q - 3.689}\frac{h^2t^3}{l^3} \tag{4.23}$$

Equation 4.23 indicates that the energy loss in triangular meshes diminishes as more and more springs are added.

4.7 Effect of Number of Cells on Maximum Stress

Similar to how the energy loss in the metamaterial was calculated, a similar procedure can be done on the maximum stresses found in the structure. Doing so results in equation 4.24.

$$\sigma_{max} = \frac{m^2}{n^2}\pi^2\frac{Eth}{l^2}\left(\frac{4}{3} + \frac{4}{3Q} + \frac{4}{27}\sqrt{\frac{192}{\pi^2} + 162 - 972\frac{1}{Q^2}}\right) \tag{4.24}$$

Equation 4.24 shows that if the structure is uniformly reduced ($m = n$) the stresses remain the same. Otherwise, they increase with more columns being added and decrease with more rows being added. The additional rows decrease the overall height of the structure, thus resulting in a lower h found in equation 1.14. This reduction in h decreases the overall stress. A similar methodology can be applied to t and l.

4.8 Conclusion

Scale 4.4 shows how the primary variables of the structure will scale the energy lost by the system. From this scale, a surrogate model of the structure was produced in equation 4.16. This function was expanded to see how the system behaves as a

metamaterial in equations 4.21 and 4.23. Lastly, a similar approach was done to examine how the stress scaled within the structure. Now that the variables and the effects are known, the results obtained by this chapter may be used directly in optimization or be used to help select variable ranges in optimization.

Chapter 5

Optimization

5.1 Introduction

With the system's behavior understood, optimization of the system can now take place. The system has 5 variables: E, b, h, t, and l. These parameters will be optimized to produce a structure with the highest E_{loss} values. This chapter will begin by discussing the optimization procedure and discuss key portions of the MATLAB® code. For optimization, first a single beam will be optimized, followed by a structure of these beams. For the structure optimization, it is assumed that the boundary conditions found in equation 1.4 are enforced.

5.2 Optimization

To optimize the structure, the objective is to maximize the energy lost by the system, equation 3.1. The constraints are the geometric constraints defined by the problem, and the stress constraint found in equations 1.14 and either 3.9 and 3.10 for rectangu-

lar meshes, or 3.12 for triangular meshes, and the ratio of h to t found in equation 1.15. Because the surrogate model was produced on the range $Q = [3, 30]$, the constraint on Q will be set to 3.

For rectangular meshes:

Maximize:

$$E_{loss} = \sum_{j}^{m} n \times E_j$$

Subject to:

$$\sigma_{yield} > \begin{cases} \pi^2 \frac{Eth}{l^2} \left(\frac{4}{3} + \frac{4}{3Q} + \frac{4}{27} \sqrt{\frac{192}{\pi^2} + 162 - 972 \frac{1}{Q^2}} \right) \\ \frac{1}{12} EC \frac{\pi^2}{xt_2} \left(\frac{512}{27} + \pi \frac{128}{3} \sqrt{\frac{1}{6} + \frac{16}{81}\pi^2 - \frac{1}{Q^2}} \right) \\ \frac{1}{12} EC \frac{\pi^2}{2x} \left(\frac{1}{t_2} + \frac{3lt_2}{h_2^3} \right) \left(\frac{512}{27} + \pi \frac{128}{3} \sqrt{\frac{1}{6} + \frac{16}{81}\pi^2 - \frac{1}{Q^2}} \right) \end{cases}$$

$$Q > 3$$

For triangular meshes:

Maximize:

$$E_{loss} = \sum_{j}^{m} j \times E_j$$

Subject to:

$$\sigma_{yield} > \begin{cases} \pi^2 \frac{Eth}{l^2} \left(\frac{4}{3} + \frac{4t}{3h} + \frac{4}{27} \sqrt{\frac{192}{\pi^2} + 162 - 972 \frac{1}{Q^2}} \right) \\ \frac{1}{12} \frac{Ebht^3}{l^3} \frac{1}{t_2 b} \left(\frac{512}{27}\pi^2 + \pi^3 \frac{128}{3} \sqrt{\frac{1}{6} + \frac{16}{81}\pi^2 - \frac{1}{Q^2}} \right) \times \binom{K}{\frac{K}{2}} \frac{1}{2^K} \end{cases}$$

$$\frac{h}{t} > 3$$

$$K = n \text{ when } n \text{ is even}$$

$$K = n + 1 \text{ when } n \text{ is odd}$$

One additional function that might be of some interest is minimizing the cross-sectional area or volume of the structure. The approximate cross-sectional area of a single beam neglecting the overlap from the apex to a connector is:

$$A = t \times l + t_2 \times h_2 \tag{5.1}$$

To get the volume instead, equation 5.1 can be multiplied by b.

To find the area of the structure, it will be assumed that t changes layer to layer. With this in mind, using equation 5.1, the area for the structure becomes:

$$A = \sum_{j}^{m} (t_j \times l \times + t_2 \times h_2) \times K_{shape} \tag{5.2}$$

where K_{shape} varies based upon the mesh. For rectangles:

$$K_{rectangles} = n \tag{5.3}$$

For triangles:

$$K_{rectangles} = j \tag{5.4}$$

where n is the number of columns and m is the number of rows. Equation 5.2 can be added to the optimization outlined previously to optimize the entire structure. Just like with 5.1, the volume of the structure can be obtained by multiplying equation 5.2 by b.

Lastly, if a specific deformation pattern is required, relations 3.26 and 3.27 can be used to make the system buckle descendingly or ascendingly respectfully. Alternatively, relation 3.29 could be used to fit a specific deformation pattern. If there is a

rectangular mesh, this step may be skipped in optimization, and done in post processing to sort the layers. The triangular mesh must include this step in the optimization as the layers can not be sorted. This is because the number of springs per row changes throughout the structure.

The optimization parameters outlined above are for a metastructure. If a metamaterial is to be designed, a single cell can be optimized to produce the maximum E_{loss}. That spring's dimensions can then be scaled down to form a mesh. This can be seen in equation 4.21. If the ratio m and n remain constaint, so does the energy loss.

5.3 Optimization Scripts

To preform optimization, MATLAB® and ModeFrontier® were used. A MATLAB® script was made to model the theoretical relations, while the surrogate model was coded into the optimizer. Both scripts take in the parameters E, b, h, t, and l, and output σ_{max} and E_{loss}.

5.3.1 Key Portions of the MATLAB® Code

The equations to solve the higher order system can be found in equations 1.12 and 1.13 and the algorithm to solve the system can be seen immediately after. These equations are recreated below:

$$\frac{3}{16N^4}\Big(1+\frac{\tan^2\frac{N}{4}}{3}-\frac{\tan\frac{N}{4}}{\frac{N}{4}}\Big)F^2-\frac{4\pi^2}{(N^2-4\pi^2)^2}F+\frac{N^2}{12Q^2}-\frac{\pi^2N^2(N^2-8\pi^2)^2}{4(N^2-4\pi^2)^2}=0$$

and

$$F=\frac{N^4}{\frac{N}{4}-\tan(\frac{N}{4})}\Big(\frac{N^2}{N^2-4\pi^2}-\Delta\Big)$$

With the algorithm being:

1. Find the range N that equation 1.12 only has real solutions
2. Using the range of N, solve the corresponding F in equation 1.12
3. Use both N and F in 1.13 to solve for their corresponding Δs
4. Dimensionalize N, F, and Δ

Solving 1.12 with 1.13 provides two solutions for F and Δ. Plotting the solution directly obtained by these can be seen in figure 5.1.

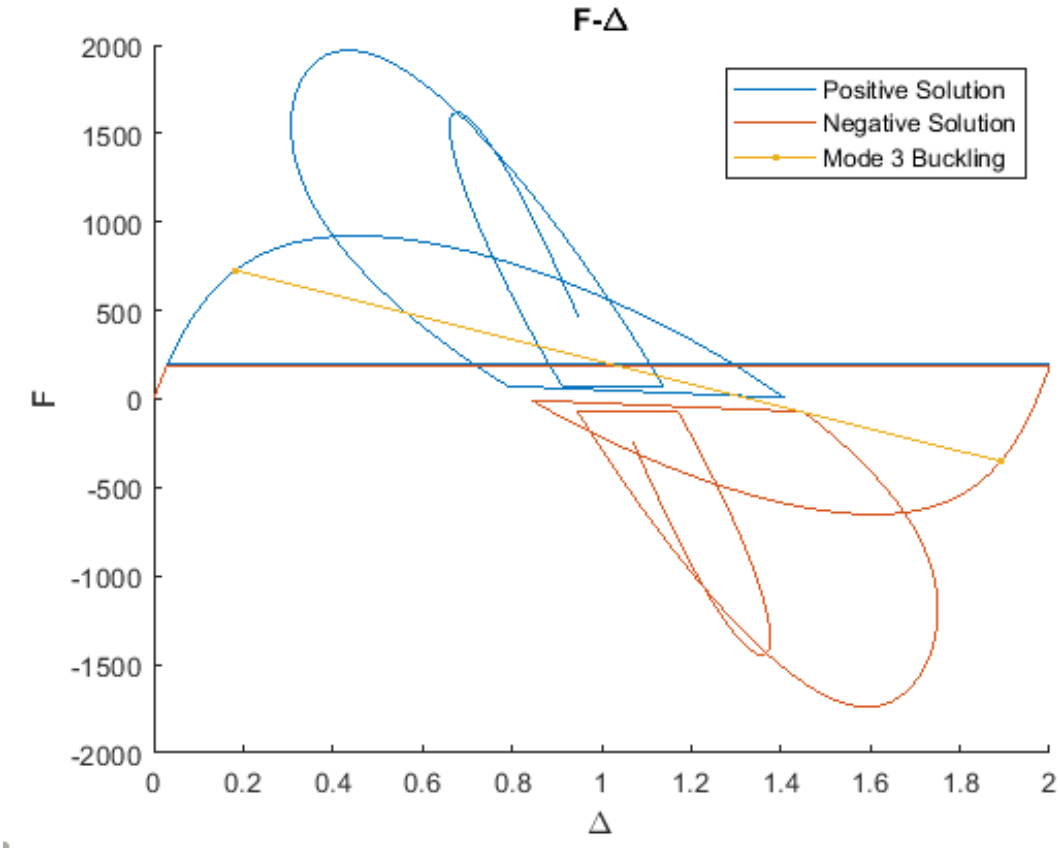

Figure 5.1: Initial $F - \Delta$ solution using Higher Modes

The portions prior to snap-through match the expected behavior, but the section in the middle is undesired. To cut these away, the following code is used:

```
1  #Remove portions exceeding the maximum displacement
2  F_1_top(Delta_1>Delta_top)=NaN;
3  F_2_top(Delta_2>Delta_top)=NaN;
4  Delta_1_top(Delta_1>Delta_top)=NaN;
5  Delta_2_top(Delta_2>Delta_top)=NaN;
6  #Remove portions exceeding the maximum force
7  Delta_1_top(F_1_top>F_top)=NaN;
8  Delta_2_top(F_2_top>F_top)=NaN;
9  F_1_top(F_1_top>F_top)=NaN;
10 F_2_top(F_2_top>F_top)=NaN;
```

Lines 2-5 clip the portions of the curve that exceed the distance of the buckling mode intersection. In the example plot seen in figure 5.2, the parameters are $E = 1, b = 1, t = 0.5, h = 3.5$, and $l = 50$. Some cases of h being exceedingly large cause the loops to extend prior to the buckling mode. In this instance, lines 2-5 would not clip the entire portion of the curve. To correct this, lines 7-10 double check the curve and eliminate the portions of the curve higher than the buckling mode. This process is repeated on the lower half of the curve. Re-running the model produces the force-displacement curve seen in figure 5.2 which matches the expected curve.

To find the areas, the plot is redimensionalized and trapezoidal integration is used to integrate the loading and unloading sections. Subtracting these two areas nets the energy lost by a single beam.

The maximum stress is given by equation 1.14. This is modeled along side the force-displacement curve to provide the stress constraint.

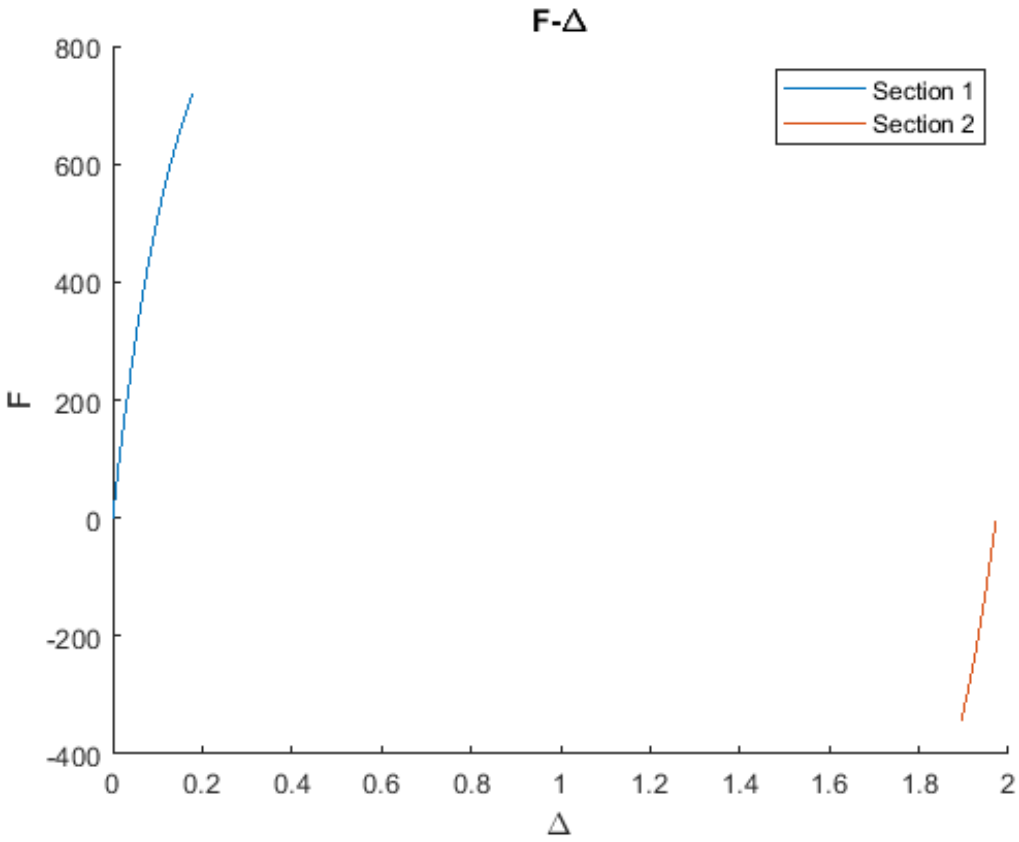

Figure 5.2: $F - \Delta$ solution using Higher Modes

5.4 Optimization Examples

To optimize the structure, MATLAB® was linked to ModeFrontier® 2017R1. This section will show the results of the MATLAB® model using the theoretical force-displacement curve and the surrogate model's results.

5.4.1 Single Spring Optimization using the Theoretical Model

For this instance, the structure is made out of Titanium Ti-6Al-4V, with $E =$ 113.8MPa and $\sigma_{yield} = 970$MPa [7]. The ranges of t, h, and l are:

$$0.1 < t < 2.0 \tag{5.5}$$

$$3.0 < h < 30.0 \tag{5.6}$$

$$30.0 < l < 500.0 \tag{5.7}$$

The diagram of the optimization from modefrontier can be seen below in figure 5.3.

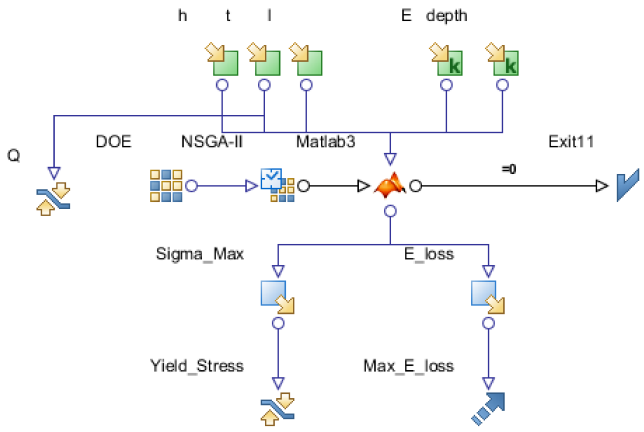

Figure 5.3: MATLAB - ModeFrontier Optimization Outline

The optimization ran for 5000 iterations and its optimal design can be seen in 5.8.

$$\begin{aligned} h &= 6.0\text{mm} \\ t &= 2.0\text{mm} \\ l &= 205.78\text{mm} \end{aligned} \tag{5.8}$$

with

$$E_{loss} = 44.639\text{Nmm}$$

$$\sigma_{max} = 970\text{MPa}$$

5.4.2 Single Spring Optimization using Surrogate Model

Using the surrogate model defined by 4.16 allows rapid simulation of the system. This model is based upon the theoretical model and should give similar results. However, due to its simplicity, the model can be run for more iterations to allow for better searching of the design space.

Running optimization on the surrogate model for 20000 iterations time on a single spring with the same constraints and limits as the previous examples nets the following dimensions:

$$\begin{aligned} h &= 6.0\text{mm} \\ l &= 205.77\text{mm} \\ t &= 2.0\text{mm} \end{aligned} \tag{5.9}$$

with

$$\begin{aligned} E_{loss} &= 44.64\text{Nmm} \\ \sigma_{max} &= 970\text{MPa} \end{aligned}$$

Alternatively, due to the simplicity of the surrogate function, solving for the maximum E_{loss} can be done with traditional optimization processes. Doing so yields:

$$\begin{aligned} h &= 6.0\text{mm} \\ l &= 205.77\text{mm} \\ t &= 2.0\text{mm} \end{aligned} \tag{5.10}$$

with

$$E_{loss} = 44.64\text{Nmm}$$

$$\sigma_{max} = 970\text{MPa}$$

It can be seen that results from 5.9 are the same as 5.10.

5.4.3 Comparison of Single Spring Optimization

Sections 5.4.1 and 5.4.2 each show separate optimization techniques. A table showing direct comparisons of the optimization results can be seen in table 5.1.

	Theory	**Surrogate**
E_{loss}(mJ)	44.639	44.64
σ_{max}(MPa)	970	970
h (mm)	6	6
t (mm)	2	2
l (mm)	205.78	205.77
Num. Iter.	5000	20000
Q=$^{h}/_{t}$	3	3
R=$^{l}/_{t}$	102.89	102.885

Table 5.1: Optimization Results

An FEA model was constructed to compare the results from the optimization. The FEA model used the same dimensions found in table 5.1. More specifically, displacement controlled was used, and it was modeled as dynamic explicit over a time frame of 1 minute. A table comparing the two can be seen in table 5.2.

		Optimization Results from	
		Theory	**Surrogate**
Re-Run with:	**Theory**	44.639	44.6352
	Surrogate	44.6439	44.640
	FEA	40.275	40.281

Table 5.2: Comparison of Results

A comparison between the force-displacement curve obtained from the theory and one obtained from FEA can be seen in figure 5.4.

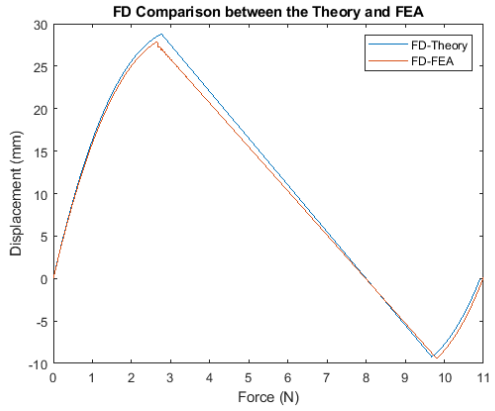

Figure 5.4: Comparison between force-displacement curves of FEA and Theory using the optimum solution obtained from theory

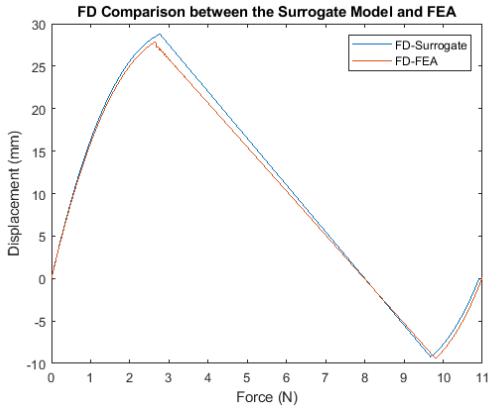

Figure 5.5: Comparison between force-displacement curves of FEA and Theory using the optimum solution obtained from the Surrogate Model

Similarly, a force-displacement comparison between the FEA and the results obtained from the surrogate model can be seen in figure 5.5. Because the surrogate model just tells the energy lost, the theoretical model was used to generate the force-displacement curves using the results from the surrogate model.

As seen in either figure 5.4 or 5.5 snap-through occurs at roughly the same displacement across all models, however the force at which snap-through occurs is less in the FEA model than in the surrogate or the theoretical model. This reduction in the force causes the energy difference seen in table 5.2.

Section 5.4.3 shows the optimization of a single spring. If this single spring was replicated throughout a structure, it would form a metamaterial. Equation 4.21 tells us that if the spring was uniformly scaled down to fill a mesh, the energy loss would remain constant.

5.5 Rectangular Metamaterial Optimization using Surrogate Model

Equations 4.21 and 4.24 show how splitting the curved beam system down into smaller beams effects energy loss and maximum stress. In this instance, a rectangular domain is considered with fixed dimensions, while the number of curved beams, n and m, are the variables. The initial curved beam system has a height of 75mm, a thickness of 5mm, a depth of 25mm, and a span of 1500mm.

The following is how the structure is to be optimized:

Maximize:

$$E_{loss} = \frac{m^4}{n^4} Eb \frac{4.251Q^2 + 3.134Q + 45.4}{Q^2 + 0.8436Q - 3.689} \frac{h^2 t^3}{l^3}$$

Subject to:

$$\sigma_{yield} > \begin{cases} \sigma_{max} = \frac{m^2}{n^2}\pi^2 \frac{Eth}{l^2}\left(\frac{4}{3} + \frac{4t}{3h} + \frac{4}{27}\sqrt{\frac{192}{\pi^2} + 162 - 972\frac{t^2}{h^2}}\right) \\ \frac{h_j}{t_j} > 3 \end{cases}$$

With:

$$\begin{aligned} n &\ \epsilon \ [1, 10] \\ m &\ \epsilon \ [1, 20] \\ t &= 5 \\ b &= 25 \\ h &= 75 \\ l &= 1500 \end{aligned}$$

Rather than running this structure through an optimizer, n and m can be algebraically solved for. Equation 4.24 says the stress is related to $({}^{m}/_{n})^2$ times the initial curved beam's stress. Meaning:

$$\frac{m}{n} \leq \sqrt{\frac{\sigma_{yield}}{\sigma_{initial}}} \tag{5.11}$$

Running the domain dimensions in the surrogate model produces initial E_{loss} and σ_{max} values.

$$\begin{aligned} E_{loss} &= 2657.2\text{mJ} \\ \sigma_{max} &= 635.3252\text{MPa} \end{aligned} \tag{5.12}$$

Using this initial stress, equation 5.11 becomes:

$$\begin{aligned} \frac{m}{n} &\leq \sqrt{\frac{970}{635.3252}} \\ &\leq 1.2357 \end{aligned} \tag{5.13}$$

If the ratio $\frac{m}{n}$ exceeds 1.2357, then the structure would yield, making 1.2357 the highest that $\frac{m}{n}$ can be. Equation 4.21 shows that the energy lost is scaled by $({}^{m}/_{n})^4$. Setting ${}^{m}/_{n}$ to be less than or equal to 1.2357 will produce the structure with the maximum energy loss. With the ranges $n\epsilon[1, 10]$ and $m\epsilon[1, 20]$, the n and m are optimized to:

$$[n, m] = [5, 6] \text{ or } [10, 12] \tag{5.14}$$

Making the energy lost in either case to be:

$$E_{loss} = 5509.9\text{mJ} \tag{5.15}$$

This E_{loss} is over twice that of a single beam as seen from 5.12.

5.6 MetaStructure Optimization

For this optimization, a metastructure will be produced. In this case, the structure is 3 rows tall and 4 cells wide. It is assumed that the spring dimensions vary only across each row, and not within each column. This leads to having a consistent l, and then three h and t values. The overall dimensions are set to the same values found in section 5.5, with $L_0 = 1500$mm, $H_0 = 75$mm, and $b = 25$mm. With a constant l, equation 4.7 gives l to be 375mm. Making the optimization outline to be:

Maximize:

$$E_{loss} = 4 \times Eb \sum_{j}^{3} \frac{4.251Q_j^2 + 3.134Q_j + 45.4}{Q_j^2 + 0.8436Q_j - 3.689} \frac{h_j^2 t_j^3}{l_j^3}$$

Subject to:

$$\sigma_{yield} > \max\left\{ \pi^2 \frac{Et_j h_j}{l^2} \left(\frac{4}{3} + \frac{4t_j}{3h_j} + \frac{4}{27}\sqrt{\frac{192}{\pi^2} + 162 - 972\frac{t_j^2}{h_j^2}} \right) \right\}$$

$$150 > h_1 - h_2$$

$$Q_j > 3$$

with:

$$t_{1,2,3} \quad \epsilon \quad [0.1, 2]$$

$$h_{1,2} \quad \epsilon \quad [10, 150]$$

$$h_3 = 150 - h_1 - h_2$$

$$b = 25$$

$$l = 375$$

$$E = 113.8\text{E}3$$

$$\sigma_{yield} = 970\text{MPa}$$

Optimizing this structure using Powell's Conjugate directions in ModeFrontier®

yields:

$$E_{loss_{total}} = 23161.6$$

$$\begin{aligned} E_{loss_{row1}} &= 2701.12 \\ E_{loss_{row2}} &= 388.556 \\ E_{loss_{row3}} &= 2701.12 \end{aligned} \tag{5.16}$$

$$\begin{aligned} \sigma_{max_1} &= 969.6 \\ \sigma_{max_2} &= 970 \\ \sigma_{max_3} &= 969.6 \end{aligned}$$

with:

$$\begin{aligned} h_1 = 17.8 \quad h_2{=}114.4 \quad h_3{=}17.8 \\ t_1 = 2.00 \quad t_2{=}0.319 \quad t_3{=}2.00 \end{aligned} \tag{5.17}$$

As seen in 5.17 the system was optimized to have two identical curved-beams and one unique curved-beam. The pair of identical beams provide the most energy loss, while the unique beam provides the least.

The results for a metastructure can be compared to that of a metamaterial in the same domain. Equation 4.6 gives the height of each spring to be 50mm. The system is still 4 cells wide, meaning the l is the same at 375mm. The maximum thickness these beams can have while remaining within the yield limit is 0.725mm. A 3x4 rectangular mesh with these dimensions gives an energy loss of:

$$E_{loss_{similarsprings}} = 2625.7\text{mJ} \tag{5.18}$$

Comparing the results for the metastructure, seen in 5.16, to the metamaterial's results shows that the metastructure with the same domain has a higher energy loss

than a similarly sized metamaterial.

5.7 Material Selection's Effect on Optimization

As mentioned in section 4.4, the material selected has a large impact on the maximum E_{loss} obtainable by the structure. More specifically, a balance must be struck between the Modulus of Elasticity of the structure and its yield strength. Table 5.3 shows the results of optimizing systems with various materials with the same constraints outlined in 5.5, 5.6, and 5.7 obtained by using the surrogate model. Only elastic behavior was modeled.

	E_{loss} **(mJ)**	E **(MPa)**	σ_{yield} **(MPa)**	h **(mm)**	t **(mm)**	l **(mm)**	b **(mm)**
Ti-Al6-4V	44.64	113.8e3	970	6	2	205.77	
CoCr	14.42	210e3	560	6	2	367.89	
Al 6061 T6	8.71	68.9e3	276	6	2	300.16	
PolyCarbine	5.24	3.1e3	70	6	2	126.42	
AISI 1006 Steel	5.06	206e3	285	5.87	1.96	500	
Stainless Steel	2.76	193e3	215	5.27	1.76	500	1
PLA	2.46	3.5e3	35.9	6	2	169.44	
Bronze, SAE 40	2.13	93e3	125	5.79	1.93	500	
Titanium, Ti	2.03	116e3	140	5.49	1.83	500	
Nylon 11	1.76	6.8e3	44	6	2	236.17	
Copper	3.3E-5	110e3	33.3	3	0.79	500	

Table 5.3: Material Selection's impact on E_{loss}

Table 5.3 shows that materials with a high E and a high σ_{yield} allow for structures with higher energy loss.

Chapter 6

Conclusion

6.1 Conclusion

Overall the research presented in this document shows that a metamaterial or metastructure can be created out of elastic materials that provides energy loss.

Chapter 2 discusses how the system loses energy, how that energy is transformed, and how to calculate it. By obtaining the force-displacement curves of the structure under loading, the areas contained by these portions can be discovered. The difference between these sections relates to how much energy is dissipated. Due to the suddenness of the translation, the energy is dissipated in the form of vibrations.

Moving beyond a single cell, chapter 3 investigates how a network of these springs will work as a whole. Section 3.2 shows how to calculate the energy loss of a mesh of these cells. Section 3.4 tells how the springs deform in that network. Lastly, in order for the structure to be constructed, section 3.3 relates how to design portions connecting each spring to one another.

With the structure's intricacies understood, understanding how the structure's dimensions effect the E_{loss} is helpful in setting the bounds of the optimization. How the E_{loss} scales is obtained by scale 4.4. Moving beyond a single spring to a mesh of springs, a relation of the thickness of the springs to the number of springs in x-y is obtained by equation 4.9. Lastly, the scale is used to construct a surrogate model seen in 4.16 to be used later in optimization. This scale was found in equation 4.16, and accurately predicts the energy lost by the system.

Speaking of optimization, chapter 5 begins by discussing how the optimization is performed, and the three systems used to perform it: FEA, Theoretical Relations, and the Surrogate Model. Optimizations of a single spring using each of the three methods are then compared and discussed. Using the surrogate model, a rectangular mesh is then optimized and discussed.

6.2 Future Work

6.2.1 Physical Parts

This research solely focused on understanding how energy is lost by the system, calculating it, then optimizing it. Because of this, there were no physical models produced and tested. An important piece of work is to physically produce one or several of these parts to test and verify the simulation results.

The individual springs could be tested to verify the theoretical energy loss and fatigue limits. The same can be said for a mesh of these springs. A physical test can also be performed to test the deformation pattern of the structure.

6.2.2 Mesh Combinations

Chapter 3 investigated the system behavior of a network of these springs in either a rectangular or triangular pattern. However,these meshes themselves can be combined to produce more complex meshes. Take figure 6.1 for example. It features three rectangular meshes combined to form one whole mesh with a hole in the bottom center. The purple dotted lines mark the outline of each rectangular mesh. In this example, each mesh is 2 springs tall. Mesh 1 is 4 wide, 2 is 1 wide, and 3 is 2 wide. This mesh can be useful to produce a maintenance opening. However,the removal of the spring marked in green can cause some issues when loading. Exactly how this structure behaves and how to predict and mitigate undesired deformation is an area of future study.

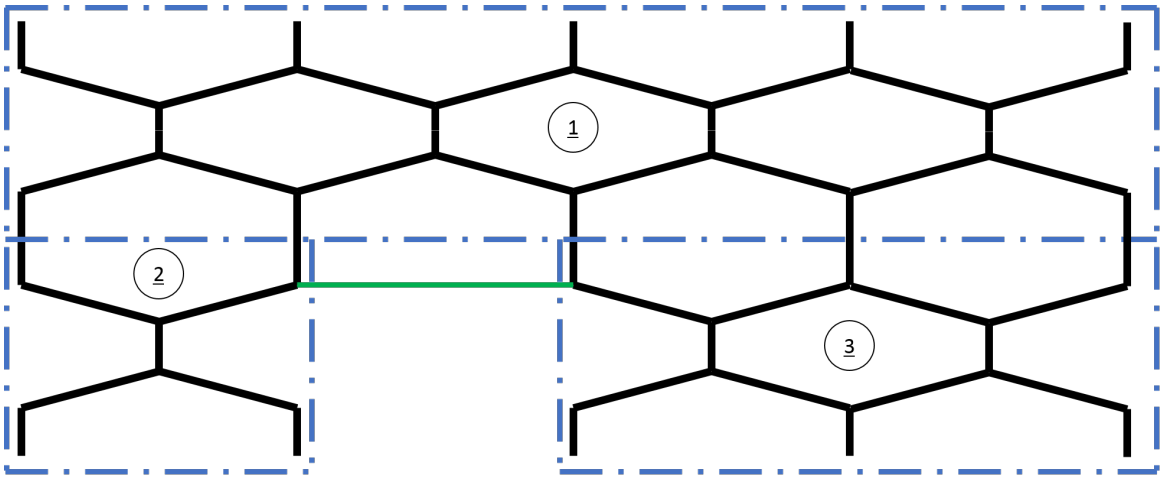

Figure 6.1: Assembly of Mesh Example.

6.2.3 Mesh with Varying l

The meshes studied in this paper make the assumption that the spring's span, l, remains constant throughout the structure. If the span is a variable, this would open up the design space possibly leading to better structures. However, by varying the

span, this opens up alignment issues that need to be dealt with.

Preliminary analysis showed strange twisting behavior present in the structure when the spans were varied. This is likely due to snap-through occurring at varying forces throughout the structure. If a mesh with varying l is desired, additional investigation is necessary.

Appendix A

E_{loss} with varying $E, b, h, t,$ and l

To get the scale of the function, five tests were performed. In each of these tests, one variable from E, b, h, t, and l was varied, and the others were held constant. Running multiple tests shows how each individual variable scales the E_{loss}.

Varying E:

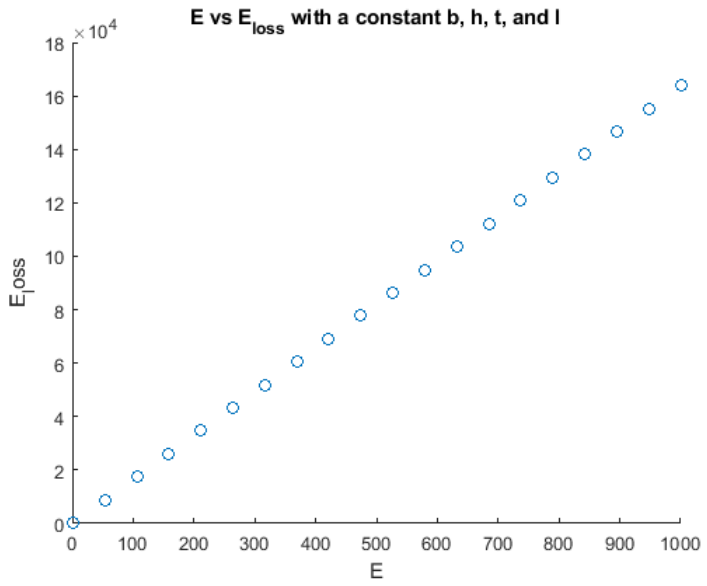

Figure A.1: E_{loss} as a function of E

Varying b:

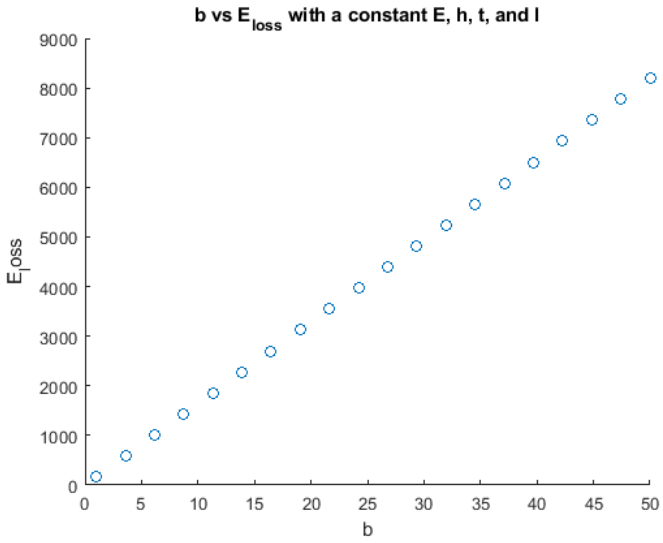

Figure A.2: E_{loss} as a function of b

Varying h:

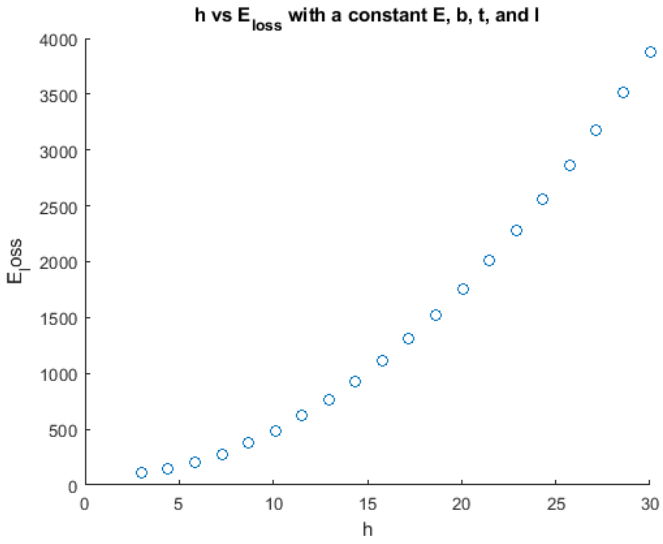

Figure A.3: E_{loss} as a function of h

Varying t:

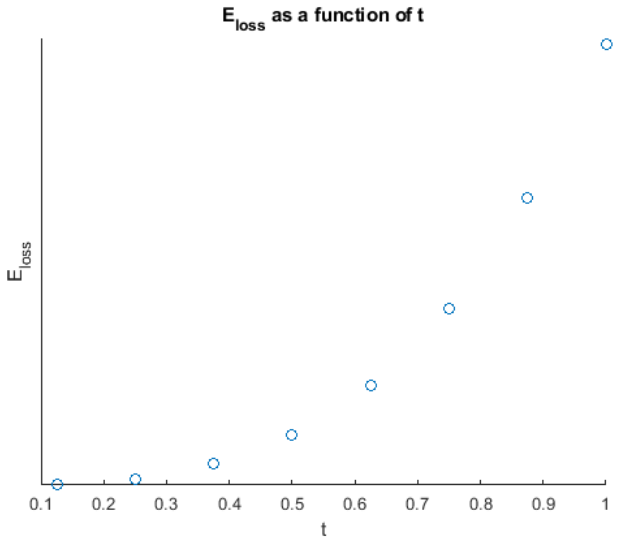

Figure A.4: E_{loss} as a function of t

Varying l:

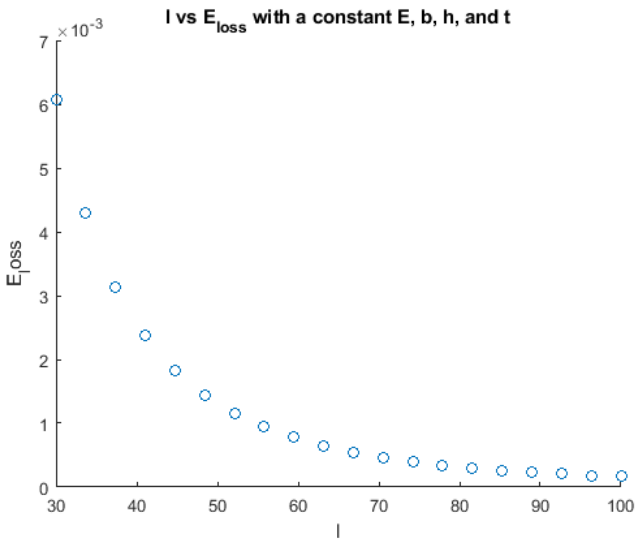

Figure A.5: E_{loss} as a function of l

Appendix B

Dimensions for Theory and Surrogate models.

Using a uniform Latin hypercube on the range $^{h}/_{t} = [3, 30]$ and $^{l}/_{t} = [30, 500]$ produces:

H	**L**	**Theory**	**Surrogate Model**
10.2	419	6.74E-06	6.75E-06
28.9	95	4.20E-03	4.20E-03
5.69	150	5.76E-05	5.75E-05
27.9	217	3.28E-04	3.28E-04
8.75	181	6.41E-05	6.41E-05
15	485	8.84E-06	8.84E-06
3.7	286	5.13E-06	5.14E-06
21.2	132	8.52E-04	8.52E-04
25.2	383	4.89E-05	4.89E-05
12.2	72.1	1.83E-03	1.83E-03
26.5	327	8.67E-05	8.67E-05

23	301	8.43E-05	8.43E-05
24.6	375	4.97E-05	4.97E-05
20.3	255	1.09E-04	1.09E-04
8.16	465	3.36E-06	3.36E-06
18.5	30	5.58E-02	5.58E-02
16.5	227	1.03E-04	1.03E-04
6.72	103	2.27E-04	2.27E-04
16	347	2.73E-05	2.73E-05
13.5	441	9.65E-06	9.65E-06

Bibliography

[1] B. Camescasse, A. Fernandes, and J. Pouget. "Bistable buckled beam and force actuation: Experimental validations". In: *International Journal of Solids and Structures* 51.9 (2014), pp. 1750–1757. ISSN: 0020-7683. DOI: https://doi.org/10.1016/j.ijsolstr.2014.01.017. URL: http://www.sciencedirect.com/science/article/pii/S0020768314000213.

[2] Dixon M Correa et al. "Negative stiffness honeycombs for recoverable shock isolation". In: *Rapid Prototyping Journal* 21.2 (2015), pp. 193–200. DOI: 10.1108/RPJ-12-2014-0182. eprint: https://doi.org/10.1108/RPJ-12-2014-0182. URL: https://doi.org/10.1108/RPJ-12-2014-0182.

[3] David A. Debeau, Carolyn C. Seepersad, and Michael R. Haberman. "Impact behavior of negative stiffness honeycomb materials". In: *Journal of Materials Research* 33.3 (2018), pp. 290–299. DOI: 10.1557/jmr.2018.7.

[4] Vassili Fedotov. "Metamaterials". In: *Springer Handbook of Electronic and Photonic Materials*. Ed. by Safa Kasap and Peter Capper. Cham: Springer International Publishing, 2017, pp. 1–1. ISBN: 978-3-319-48933-9. DOI: 10.1007/978-3-319-48933-9_56. URL: https://doi.org/10.1007/978-3-319-48933-9_56.

[5] Samuel Franklin et al. "Design of Meta-material Tank Track System with Experimental Testing and Sensitivity Analysis of Additively Manufactured Metamaterial Backer Pads". MA thesis. Clemson University, Aug. 2018.

[6] Hussein Hussein et al. "Modeling and Stress Analysis of a Pre-Shaped Curved Beam: Influence of High Modes of Buckling". In: *International Journal of Applied Mechanics* 7.4 (2015). DOI: https://doi.org/10.1142/S1758825115500556.

[7] ASM Aerospace Specification Metals Inc. *Titanium Ti-6Al-4V (Grade 5), Annealed*. URL: http://asm.matweb.com/search/SpecificMaterial.asp?bassnum=mtp641 (visited on 02/28/2019).

[8] Mad Physics. *Hysteresis and Rubber Bands*. URL: http://www.madphysics.com/exp/hysteresis_and_rubber_bands.htm (visited on 03/24/2008).

[9] Jin Qiu, Jeffrey H. Lang, and Alexander H. Slocum. "A Curved-Beam Bistable Mechanism". In: *Journal of MicroElectromechanical Systems* 13.2 (2004), pp. 137–146. DOI: http://dx.doi.org/10.1109/JMEMS.2004.825308.

[10] Zachary Satterfield et al. “Unit Cell Synthesis for Design of Materials With Targeted Nonlinear Deformation Response”. In: *Journal of Mechanical Design* 139 (Sept. 2017). DOI: 10.1115/1.4037894.

[11] James Surjadi et al. “Mechanical Metamaterials and Their Engineering Applications”. In: *Advanced Engineering Materials* (Jan. 2019). DOI: 10.1002/adem.201800864.